

Flat-plane based double-counting free and parameter free many-body DFT+U

Andrew C. Burgess¹ and David D. O'Regan^{1,*}

¹*School of Physics, Trinity College Dublin, The University of Dublin, Ireland*

(Dated: November 14, 2024)

Burgess et al. have recently introduced the BLOR corrective exchange-correlation functional that is, by construction, the unique simplified rotationally-invariant DFT+ U functional that enforces the flat-plane condition separately on each effective orbital of a localized subspace. Detached from the Hubbard model, functionals of this type are both double-counting correction free and, when optimized in situ using appropriate error quantifiers, effectively parameter free. They are as computationally undemanding as conventional DFT+ U functionals. In this work, the extension of the BLOR functional to address many-body errors (mBLOR) is derived. The mBLOR functional is built to enforce the flat-plane condition on the entire subspace, rather than on each orbital individually. It depends solely on the total subspace occupancy and spin magnetization, bringing consistency with how Hubbard U and Hund J values are typically calculated, and very low complexity. In this way inter-orbital errors are corrected on the same footing as the single-particle ones. Focusing on exact test cases with strong inter-orbital interactions, the BLOR and mBLOR functionals were benchmarked against contemporary DFT+ U functionals using the total energy extensivity condition on stretched homo-nuclear p-block dimers that represent various self-interaction and static-correlation error regimes, namely singlet N_2 & F_2 , non-spin polarized O_2 , and doublet Ne_2^+ . The BLOR functional outperformed all other DFT+ U functionals tested, which often act to increase total-energy errors, yet it still yielded large errors in some systems. mBLOR instead yielded low energy errors across all four strongly-correlated dimers, while being constructed using only semi-local approximation ingredients. As mBLOR would not otherwise introduce a band-gap correction in the manner that is a desirable feature of DFT+ U , we developed a cost-free technique to reintroduce it automatically by moving the functional's unusual explicit derivative discontinuity into the potential. With this in place, mBLOR is the only known DFT+ U functional that opens the bandgap of stretched neutral homo-nuclear dimers without the aid of unphysical spin-symmetry breaking.

Density Functional Theory (DFT) [1–4] is a central element of modern-day condensed matter physics and materials chemistry. It is a leading method for the prediction of the electronic, magnetic and crystallographic structures of solid state materials thanks largely to its favorable balance between predictive accuracy and computational efficiency. This balance strongly depends on the choice of exchange-correlation (XC) approximation.

However, current XC approximations such as the Local Spin Density Approximations, (LSDAs) [5–9], Generalized Gradient Approximations (GGAs) [10–14], meta-GGAs [15–19] and hybrid functionals [20, 21] are all known to fail in cases where the electronic system contains one or more isolated, localized subsystems. To mention a prototypical example, this failure was investigated by Perdew for the quintessential Mott insulator [22], the hydrogen lattice at the infinite atomic separation limit, which has an ionization energy of 13.6 eV and a bandgap of 12.8 eV. Perdew showed that the LSDA underestimates the ionization energy by approximately 46% and, moreover, that it spuriously predicts the hydrogen lattice to be metallic.

Such failures of the LDA, GGAs, meta-GGAs and hybrid functionals are also well documented for the dissociation of molecular dimers [23–25] and in the prediction of 3d transition metal oxides, where in both cases va-

lence electrons remain partially or completely localized on atomic sites.

I. DOUBLE-COUNTING FREE TREATMENT OF LOCALIZED ELECTRONIC STATES

In the case of electronic systems with isolated localized subsystems, the energy of each isolated localized state should obey the tilted plane condition [26] in the limit where the interaction between the localized state and the bath (the rest of the electronic system) is negligible, or more generally, when the subspace-bath interaction energy varies linearly with spin resolved subspace occupancy. Standard XC functionals however, will exhibit spurious curvature in the energy of each isolated, localized state. This will result in erroneous total energies of the global system whenever the isolated subspaces have non-integer values of subspace electron count N and subspace magnetization M . These errors in the total energy will occur even at integer values of global electron count N_{tot} and magnetization M_{tot} [27]. We refer to these energy errors as localized many electron self interaction errors and localized static correlation errors [28, 29] to distinguish them from their global analogues [30].

Noting the qualitative failures of standard XC approximations when simulating Mott insulators, Anisimov et al. [31] proposed supplementing such XC approximations with an additional electronic interaction term inspired by

* david.o.regan@tcd.ie

the Hubbard model [32],

$$E_{\text{int}} = \frac{U}{2} \sum_{mm'\sigma} n_{m\sigma} n_{m'\bar{\sigma}} + \frac{U-J}{2} \sum_{\substack{mm'\sigma \\ m \neq m'}} n_{m\sigma} n_{m'\sigma}, \quad (1)$$

which explicitly depends on the spin resolved occupancy $n_{m\sigma}$ of each orbital m in the localized subspace. U and J refer to the Hubbard U and Hund's J interaction parameters which need to be chosen or preferably evaluated [33–40], in advance. The inter-electron interactions of Eq. 1 however, are already accounted for to a less favourable extent by the original XC functional that the Hubbard-like interaction term is designed to supplement. This necessitates the use of a double counting correction scheme. The inter-electron interaction and double counting scheme together form a DFT+ U -type functional [28, 31, 37, 41–55]. Over the past three decades numerous double counting correction schemes have been developed including the spin polarized and non-spin polarized analogues of the around mean field [31, 42] and fully localized limit [41, 42] double counting schemes. In practical applications, the predicted physical and chemical properties of a material can strongly depend on the choice of double counting scheme [56, 57]. Despite this strong dependency, DFT+ U -type functionals enjoy widespread application, most notably in high throughput material screening [58–61], which can require thousands of DFT+ U -type calculations to be executed.

Developing a DFT+ U -type functional that yields reliable total energies and bandgaps is thus of crucial importance. Improved understanding in recent years of exact conditions that apply to the atomic limit has given the opportunity to design DFT+ U that encode those, without adding complexity, rather than invoking approximate double-counting corrections [28]. Meanwhile, incorporation from the field of quantum chemistry of the use of test systems for which exact total energies, or at least exact total-energy differences, are available, enables the stringent determination of the viable class of functional forms of a given complexity level [28, 47, 48]. Departing entirely from the Hubbard model and hence circumventing the introduction of a double-counting correction, in this work we develop a DFT+ U -type functional whose form is entirely based upon exact conditions in DFT. Specifically, we focus on the regime in which the DFT+ U subspaces are relatively weakly interacting with the remainder of the system, so that they harbor the exact flat-plane (or more generally tilted-plane) condition, and where their deviations from that condition, many-body self-interaction error (SIE) and many-body static-correlation error (SCE), are treated in a subspace-averaged fashion in the usual pragmatic, cost-effective manner of DFT+ U .

II. EXACT CONDITIONS IN DFT

The poor performance of most XC functionals in the prediction of electronic systems with partially or completely localized states, can be largely attributed to their breaking of certain physical conditions [62] that the exact XC functional is known to obey, the best known among which is the piecewise linearity condition with respect to electron count [63–65]. The total ground-state energy of a system with non-integer electron count N_{tot} , must be a linear interpolation of the ground-state energies of the same system with integer values of electron count N_0 and $N_0 + 1$,

$$E_v[N_{\text{tot}}] = \omega E_v[N_0] + (1 - \omega) E_v[N_0 + 1], \quad (2)$$

$$\text{where } N_{\text{tot}} = \omega N_0 + (1 - \omega)(N_0 + 1), \quad 0 \leq \omega \leq 1.$$

This exact condition was originally explicated by Perdew et al. [63] assuming the convexity condition with respect to electron count is satisfied,

$$2E_v[N_{\text{tot}}] \leq E_v[N_{\text{tot}} - 1] + E_v[N_{\text{tot}} + 1]. \quad (3)$$

Recently the convexity condition has been proven to be true for all electronic systems within DFT [66], whenever the density functional is (1) exact for all v -representable densities, (2) size-consistent, and (3) translationally invariant.

An analogous exact condition of equal importance is the piecewise linearity condition with respect to magnetization [26, 67, 68]. The total ground-state energy of a system with non-integer magnetization M_{tot} but integer electron count N_0 , must be a linear interpolation of the ground-state energies of the same system with integer values of magnetization M_i and M_j ,

$$E_v[N_0, M_{\text{tot}}] = \omega E_v[N_0, M_i] + (1 - \omega) E_v[N_0, M_j], \quad (4)$$

$$M_{\text{tot}} = \omega M_i + (1 - \omega) M_j, \quad M_i, M_j \in \mathbb{Z} \quad \& \quad 0 \leq \omega \leq 1.$$

These two exact conditions have been combined and extended to give the flat plane condition [64, 67, 69–78], or more generally the tilted plane condition [26, 79] when the full range of possible magnetization states are considered. The tilted plane condition requires that the exact $E_v[N_{\text{tot}}, M_{\text{tot}}]$ curve for any finite electronic system is composed of a tiled surface with vertices occurring at certain integer values of electron count and magnetization, with derivative discontinuities along the edges of each tile. Several functionals have been developed that either fully or partially satisfy the flat or tilted plane condition [28, 47, 48, 76, 80–87], or help mitigate deviations from it. The exact flat plane condition for the helium atom and neon atom is illustrated in Fig. 1.

LDA, GGAs, meta-GGAs and hybrid functionals do not obey the tilted plane condition and instead exhibit a spurious curvature in the total energy with respect to N_{tot} and M_{tot} . In the literature, this erroneous behaviour is typically referred to as Many Electron Self Interaction Error [23, 89] and Static Correlation Error [68], respectively.

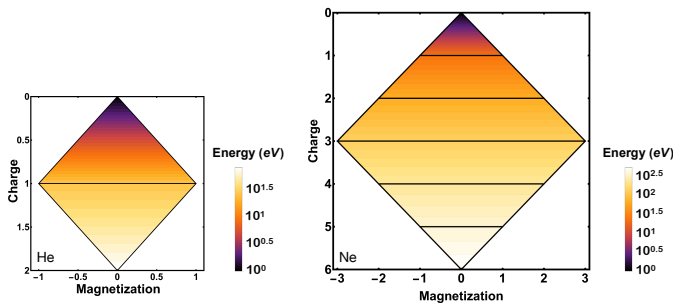


FIG. 1. The projection of the $E_v[N_{\text{tot}}, M_{\text{tot}}]$ curve of the helium atom (left) and neon atom (right) onto the $N_{\text{tot}} - M_{\text{tot}}$ plane. For simplicity, highly charged and highly magnetized states are omitted. The total energy varies linearly across each plane, which are outlined in black. The total energy values are based on available experimental NIST reference data [88] and are given relative to the lowest energy state of the respective neutral atom which is set to 1 eV. Energy contour lines are plotted at intervals of $10^{0.05x}$ eV. In the BLOR functional [28], the spin-dependent occupancy of each DFT+ U subspace spatial orbital can be thought of as being separately mapped, conceptually, to its own possibly-tilted helium atom (left) exact energy model. In the introduced mBLOR functional, and taking the example of p-orbital based subspaces, the spin-dependent occupancies of all three subspace spatial orbitals are together mapped to a combined possibly-tilted neon 2p subshell (right) exact energy model.

III. THE BLOR FLAT-PLANE CONDITION BASED DFT+ U FUNCTIONAL

Burgess, Linscott, and O’Regan recently developed the BLOR DFT+ U functional [28], which is defined to enforce the flat plane condition on each orbital of a localized subspace, thus dispensing with the need to invoke the Hubbard model or a double counting correction scheme.

$$E_{\text{BLOR}} = \begin{cases} \frac{U^\uparrow + U^\downarrow}{4} \text{Tr}[\hat{N} - \hat{N}^2] & + \frac{J}{2} \text{Tr}[\hat{M}^2 - \hat{N}^2] & + \frac{U^\uparrow - U^\downarrow}{4} \text{Tr}[\hat{M} - \hat{N}\hat{M}], & \text{Tr}[\hat{N}] \leq \text{Tr}[\hat{P}]. \\ \frac{U^\uparrow + U^\downarrow}{4} \text{Tr}[(\hat{N} - \hat{P}) - (\hat{N} - \hat{P})^2] & + \frac{J}{2} \text{Tr}[\hat{M}^2 - (\hat{N} - 2\hat{P})^2] & + \frac{U^\uparrow - U^\downarrow}{4} \text{Tr}[\hat{M} - \hat{N}\hat{M}], & \text{Tr}[\hat{N}] > \text{Tr}[\hat{P}], \end{cases} \quad (5)$$

where the subspace occupancy and magnetization operators can be expressed in terms of the spin-resolved subspace occupancy operators $\hat{N} = \hat{n}^\uparrow + \hat{n}^\downarrow$ and $\hat{M} = \hat{n}^\uparrow - \hat{n}^\downarrow$. The spin-resolved subspace occupancy operator is $\hat{n}^\sigma = \hat{P}\hat{\rho}^\sigma\hat{P}$, where $\hat{\rho}^\sigma$ is the spin- σ Kohn-Sham density operator and \hat{P} is the subspace projection operator.

By enforcing the tilted plane condition separately on each orbital of the subspace, the BLOR functional acts to enforce a helium like flat plane condition, as depicted in Fig. 1, on each of the $\text{Tr}[\hat{P}]$ orbitals of the subspace. Following standard practice in DFT+ U , this orbital re-

solved functional is then applied using subspace-averaged U and J parameters. This amounts to an approximation or inconsistency, but perhaps more importantly to the neglect of inter-orbital corrections within the subspace, and hence the restriction to single-orbital rather than many-body SIE and SCE.

The functional form of BLOR is uniquely specified by its definition, as proven in Supplementary Material S-II of Ref. 28. In order to enforce the localized tilted plane condition, the spin resolved Hubbard U^σ parameter must be defined as the spurious curvature (in the physics sense meaning second derivative) of an appropriately defined energy with respect to spin resolved subspace occupancy n^σ (at fixed $n^{\bar{\sigma}}$, where $\bar{\sigma}$ is the spin opposite to σ). Similarly the magnitude of the Hund’s J parameter must be defined as the spurious curvature of an appropriate energy with respect to subspace spin-magnetization (at fixed subspace occupancy). We note that localized spurious energy curvatures with respect to charge are closely related, albeit somewhat different technically, to the violation of the generalized DFT Koopmans’ theorem endemic to practical approximate functionals. The currently most practical comprehensive remedy for the latter, in in-situ corrective form, are the Koopmans compliant functionals detailed, e.g., in Refs. 90–92.

The BLOR functional was found to yield highly accurate total energies for s-valence molecular systems at large separation lengths, namely H_2 , He_2^+ , Li_2 , Be_2^+ and the triplet H_5^+ ring, with relative energy errors below 0.6%. These same molecular systems suffer from relative energy errors as high as 8.0% at the raw DFT level, using the Perdew-Burke-Ernzerhof (PBE) approximation. Use of current standard DFT+ U -type functionals such as Dudarev’s 1998 Hubbard functional [44] or Liechtenstein’s 1995 Hubbard functional [43] (the two corrective functionals are equivalent in the case of s-valence species) often significantly worsened the raw approximate DFT (PBE functional) total energy, with relative energy errors as high as 20.5%. In the case of multi-orbital subspaces, the BLOR functional was designed to enforce the localized tilted plane condition separately on each orbital of the subspace, and is defined by

functional effectively enforces one neon-like flat plane condition (for the example of a p-orbital subspace; for d-orbitals we would refer to zinc) as opposed to enforcing a set of $\text{Tr}[\hat{P}]$ separate helium like flat plane conditions. Before explicating this alternative DFT+ U -type functional in full, we will first elaborate on how these subspace averaged U and J parameters are evaluated.

IV. HUBBARD AND HUND PARAMETERS

Measuring the spurious curvature in the energy with respect to occupancy, while fixing the spin-magnetization, would in principle require cumbersome and often ill-conditioned self-consistent constrained DFT calculations. Instead, one can directly evaluate the corrective parameters U and J based on first-order partial derivatives of the spin-resolved, subspace averaged Hartree and exchange-correlation (Hxc) potential,

$$v_{Hxc}^\sigma = \text{Tr} \left[\hat{P} \frac{\delta E_{Hxc}^{\text{total}}}{\delta \rho^\sigma} \right] / \text{Tr}[\hat{P}], \quad (6)$$

where E_{Hxc}^{total} is the total Hxc energy of the system and \hat{P} is the subspace projection operator. Using v_{Hxc}^σ , we can define the spin-resolved subspace Hxc interaction

$$f^{\sigma\sigma'} = \left. \frac{\partial v_{Hxc}^\sigma}{\partial n^{\sigma'}} \right|_{n^{\bar{\sigma}'},} \quad (7)$$

where $n^{\sigma'}$ is the spin σ' subspace occupancy. This is known as the minimum-tracking linear response method [33, 93–95]. Within this formalism, the spin resolved Hubbard parameters for BLOR (or mBLOR) can be set as the diagonal elements of the Hxc interaction, namely as

$$U^\sigma = f^{\sigma\sigma}. \quad (8)$$

The Hund's J parameter is defined as the spurious curvature in the interacting part of the energy with respect to magnetization. Within the minimum-tracking linear response formalism it is normally defined as

$$J = -\frac{1}{2} \frac{dv_{Hxc}^\uparrow - dv_{Hxc}^\downarrow}{d(n^\uparrow - n^\downarrow)}. \quad (9)$$

However, this derivative with respect to magnetization should, for functionals such as BLOR and mBLOR, be evaluated at fixed total occupancy. This variation can be calculated very conveniently using the simple 2×2 method [33], where it is given by

$$J = -\frac{1}{4}(f^{\uparrow\uparrow} - f^{\uparrow\downarrow} - f^{\downarrow\uparrow} + f^{\downarrow\downarrow}). \quad (10)$$

Similarly, within the minimum-tracking linear response formalism the spin-independent Hubbard U parameter is usually defined as

$$U = \frac{1}{2} \frac{dv_{Hxc}^\uparrow + dv_{Hxc}^\downarrow}{d(n^\uparrow + n^\downarrow)} \quad (11)$$

and, again, there exists an analogous simple 2×2 variant (particularly, but not necessarily only for use with flat-plane condition based functionals),

$$U = \frac{1}{4}(f^{\uparrow\uparrow} + f^{\uparrow\downarrow} + f^{\downarrow\uparrow} + f^{\downarrow\downarrow}). \quad (12)$$

Thus, the Hubbard U (and Hund's J) parameters are typically evaluated as subspace averaged localized many-body SIE (and SCE) strengths, or subspace averaged interaction strengths of a specific type, depending on the reader's perspective. Despite this subspace averaging, the U and J parameters are typically employed in orbitally resolved DFT+ U -type functionals, such as the original BLOR functional of Eq. 5 or Dudarev et al.'s functional [44],

$$E_u = \frac{U - J}{2} \sum_{\sigma mm'} n_{mm'}^\sigma \delta_{mm'} - n_{mm'}^\sigma n_{m'm}^\sigma. \quad (13)$$

These subspace averaged U and J parameters can in principle be decomposed into orbitally resolved contributions

$$f_{mm'}^{\sigma\sigma'} = \left(\frac{\partial v_{Hxc}^{m\sigma}}{\partial n_{m'\sigma'}} \right), \quad (14)$$

although we emphasize that this decomposition is not performed in this study. In an atomic subspace of orbital angular momentum quantum number l , for every one on-diagonal intra-orbital term $f_{mm}^{\sigma\sigma'}$ contributing to the subspace averaged U and J parameters there will be $2l$ off-diagonal inter-orbital terms $f_{mm'}^{\sigma\sigma'}$, where $m \neq m'$. Due to the contributions from these inter-orbital terms $f_{mm'}^{\sigma\sigma'}$, it is inconsistent to use such subspace averaged U and J parameters in an orbitally resolved DFT+ U -type functional. This approximation will tend to ascribe all the measured many-body localized SIE and SCE to the inter-orbital (single-particle) terms, likely over-correcting them, while neglecting the numerous inter-orbital corrective terms. How great an issue this is in practice is likely dependent on the system under study and the choice of subspace projection. It seems likely to be more problematic, for the accuracy of the total energy, when there are more than one significantly partially occupied subspace spin-orbitals. This inconsistency can, of course, be resolved by following the long-known route of evaluating orbitally resolved corrective parameters [37, 96–98] or alternatively, one could develop a non-orbitally resolved DFT+ U -type functional designed to mitigate errors or account for on-site interactions associated with the subspace as a whole as opposed to each orbital separately. It is the later of these two options which we choose to pursue in this study. Unlike the orbitally resolved parameter approach, this one does not present challenges in maintaining a functional form that is invariant under unitary transformations of the orbitals. In principle, this latter approach could be applied to subspaces that are not orbital based at all, but for example defined by a weight function in real space, which might prove most helpful in orbital-free DFT.

V. FLAT-PLANE BASED FUNCTIONAL THAT INCLUDES INTER-ORBITAL CORRECTIONS FOR MANY-BODY ERRORS: MBLOR IN THE SPIN-SYMMETRIC CASE

We are now ready to derive the generalization of the BLOR functional to address many-body SIE and SCE, termed mBLOR for brevity. For simplicity, we will first consider the simpler case of a spin symmetric system whose total subspace energy satisfies

$$E[N, M] = E[N, -M]. \quad (15)$$

Here, N and M are the total subspace electron count and subspace spin-magnetization (note here that magnetization is measured in units of electrons, following convenient convention in DFT, not units of \hbar), respectively,

$$N = \sum_{\sigma m} n_{mm}^{\sigma} \quad \& \quad M = \sum_m (n_{mm}^{\uparrow} - n_{mm}^{\downarrow}). \quad (16)$$

This spin-symmetric special case simplifies matters considerably because the spurious curvature in the total subspace energy of an approximate XC functional with respect to spin up subspace occupancy n^{\uparrow} is then equal to the spurious curvature in the total subspace energy with respect to spin down subspace occupancy n^{\downarrow} . Furthermore, if $[N, M]$ is a vertex in the energy landscape, then $[N, -M]$ is a degenerate vertex in the energy landscape.

Focusing on the lowest energy magnetization states, and assuming no structure to the weak interaction with the bath for the subspace, the $E[N, M]$ surface is as shown in Fig. 1 (for the cases of single s or p-valence subspaces, the d and f cases being straightforward generalizations) assuming two criteria are satisfied.

- (a) The total energy of the subspace is strictly convex with respect to electron count, so that

$$2E[N] < E[N - 1] + E[N + 1]. \quad (17)$$

- (b) Hund's First Rule is satisfied, i.e., each orbital of the subspace is occupied singly first with electrons of parallel spin, before any double occupation occurs.

As shown in Fig. 1, the $E[N, M]$ surface in this case is composed of a series of flat planes, which meet with derivative discontinuities at integer values of electron count. The $E[N, M]$ surface in Fig. 1, displays a large number of vertices. In general we expect the approximate XC functional, that BLOR is designed to supplement, to yield accurate total energies for atomic systems whenever N and M are located at vertices in the energy landscape. It is important to note that an analogous $E[N, M]$ surface to Fig. 1 will also occur for d and f valence-atoms if criteria (a)-(b) are satisfied.

In order to enforce the tilted plane condition once on a subspace that satisfies criteria (a)-(b), the corrective functional must satisfy four key conditions. It must:

1. Be a continuous function of the subspace electron count N and magnetization M .
2. Yield no correction at the vertices in the $E[N, M]$ landscape. This is desirable because approximate functionals are expected to yield accurate total energies in this case.
3. Have a constant curvature of $-U$ with respect to N . This is desirable because approximate functionals are expected to have a spurious curvature of U with respect to N due to their deviation from the tilted plane condition, and this should be subtracted off.
4. Have a constant curvature of J with respect to M . This is desirable because approximate functionals are expected to have a spurious curvature of $-J$ with respect to M (the minus is due to long-standing convention for defining J), and this should be subtracted off.

The spin-symmetric version of the mBLOR functional is the mathematically unique functional that satisfies these four conditions for a subspace that meets criteria (a)-(b), and it may be written separately for each subspace as

$$E_{\text{mBLOR}} = \begin{cases} \frac{U - J}{2} [(N - N_0) - (N - N_0)^2] + \frac{J}{2} [M^2 - N^2], & N \leq \text{Tr}[\hat{P}], \\ \frac{U - J}{2} [(N - N_0) - (N - N_0)^2] + \frac{J}{2} [M^2 - (N - 2\text{Tr}[\hat{P}])^2], & N > \text{Tr}[\hat{P}]. \end{cases} \quad (18)$$

In Eq. 18 N_0 is defined as $\lfloor N \rfloor$, where $\lfloor \cdot \rfloor$ is the floor function (the integer part). The first term on the right hand side of Eq. 18 is the many-electron self interaction error term. It mitigates the localized analogue of MSIE by re-

moving a quadratic term in N of curvature $U - J$ and replacing it with a linear term. We have used in Eq. 18 the fact that $(U^{\uparrow} + U^{\downarrow})/2 = U - J$ for spin-symmetric systems within the simple 2×2 scheme. As expected,

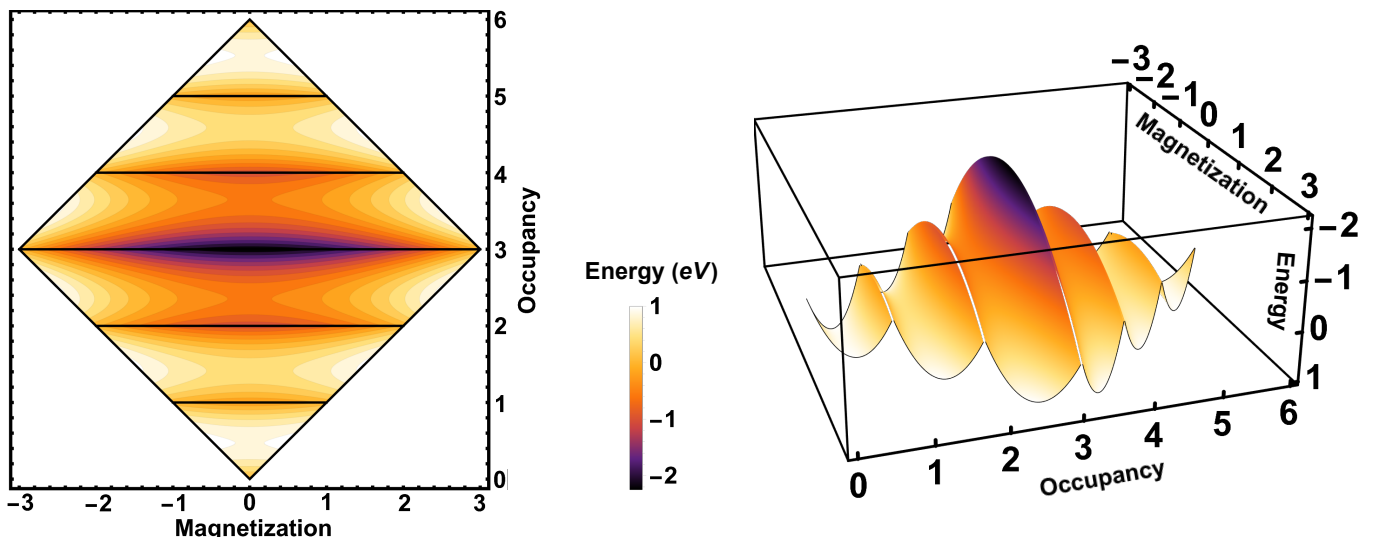


FIG. 2. Plot of the total corrective energy of the spin-symmetric mBLOR functional of Eq. 18 for a p-orbital subspace with Hubbard corrective parameters $U = 8.5$ eV and $J = 0.5$ eV. In the left-hand image energy contour lines are plotted at intervals of 0.2 eV. In the right hand image a side-on view of the same mBLOR total corrective energy surface is presented.

the MSIE term offers no correction to the total energy for systems with integer subspace occupancy. The second term on the right hand side of Eq. 18 is the static correlation error correction term, which offers no energy correction for a maximally spin polarized subspace and reaches its maximum energy correction at $M = 0$. The SCE term takes a different form depending on whether the subspace is more or less than half occupied, this is a consequence of satisfying Hund’s First Rule. We refer to these two forms as the ‘early’ and ‘late’ versions of the mBLOR functional, which should be used when $N \leq \text{Tr}[\hat{P}]$, and $N > \text{Tr}[\hat{P}]$, respectively. Beyond half occupancy, the maximum magnetization, i.e., the value of M for which the SCE term vanishes, decreases with increasing N as the orbitals of the subspace are now being filled by a second electron of the opposite spin. A plot of the spin-symmetric mBLOR corrective energy surface as a function of subspace occupancy and magnetization is presented in Fig. 2.

In passing, we note that in addition to its primary application of treating localized spin-symmetric subspaces, the mBLOR functional of Eq. 18 can also be used to mitigate approximate XC functional’s deviation from the *global* flat plane condition. In this case N and M of Eq. 18 would be replaced by the total electron count and magnetization of the finite electronic system of interest.

VI. SPIN-SYMMETRIC MOLECULAR TEST SYSTEMS

We tested the spin-symmetric mBLOR corrective functional of Eq. 18 on three spin-symmetric homo-nuclear dimers at large inter-nuclear separation lengths, namely N_2 , F_2 and (simulating its non-spin polarized triplet

ground state) O_2 . For these stretched, neutral homo-nuclear dimers, an approximately integer number of electrons localizes on each atomic site. An ambiguity therefore arises as to which integer value to use for N_0 in the mBLOR functional. Following the precedent set in the study of the stretched s-block dimers [28], we choose to set $N_0 = 2, 3$ and 4 for the stretched N_2, O_2 and F_2 molecules, respectively, so that the MSIE term in the mBLOR functional is equal to zero when the subspace occupancy is equal to that of the neutral atom and ‘plus one’ cation. This choice in values of N_0 results in the ‘early’ ($N \leq \text{Tr}[\hat{P}]$) version of the mBLOR functional being applied to the stretched N_2 system and the ‘late’ ($N > \text{Tr}[\hat{P}]$) version of the mBLOR functional being applied to the stretched O_2 and F_2 systems. The corresponding versions of the BLOR functional is applied to the stretched N_2 molecule and to the stretched O_2 and F_2 molecules. In the case of the O_2 molecule, to avoid converging to a broken-symmetry spin-polarized ground state, the occupancy of the two frontier spin up and spin down GKS orbitals were permitted, as necessary, to be degenerate with occupancy 0.5. At large inter-nuclear separation lengths, a close to integer number of electrons will localise on each atomic site, therefore these systems will suffer from negligible localized-MSIE. Being non-spin polarized molecules, the magnetization at each of the atomic sites will be equal to zero, thus for a given value of N , these systems are located at the point of maximum localized SCE. Assuming a positive in-situ measured value of J , as indeed transpires to be the case, the raw uncorrected PBE functional will thus overestimate the total energies of these stretched X_2 systems.

At the dissociated limit the total energy of the X_2

molecule, the energy extensivity condition holds, namely

$$E[X_2] = 2E[X]. \quad (19)$$

However, due to localized MSIE and localized SCE, the total energy of the X_2 molecule at large inter-nuclear separation lengths will not be equal to twice the energy of the X atom when evaluated using an approximate XC functional. The difference between these two quantities is thus an intrinsic error associated with the approximate XC functional. By contrast, the raw PBE total energy of the isolated X atom will not significantly suffer from localized MSIE or localized SCE as the system will be located at a vertex of the $E[N, M]$ energy surface by virtue of it being in the lowest energy magnetization state of the atom for a given integer value of electron count. Twice the PBE total energy of the X atom, can thus be used as our reference value. Ideally, application of a Hubbard-type corrective functional to the stretched X_2 system should mitigate this intrinsic energy error. The provided bar charts present the energy error associated with each DFT+ U -type functional, giving what are close to ideal application conditions (i.e., near the atomic limit). We define this energy error here as the energy difference between the stretched X_2 molecule evaluated with a given DFT(PBE)+ U -type functional compared to twice the PBE total energy of the X atom. Using Eq. 19 to define the exact total energy provides cancellation errors in the total energy due to the use of (very carefully designed) pseudo-potentials.

The energy results are presented in Figs. 3-5 for the stretched non-spin polarized N_2 , O_2 and F_2 molecules, respectively. The DFT+ U and DFT+($U - J$) relative errors were computed using Dudarev et al.’s 1998 functional with the effective Hubbard parameter (U_{eff}) set to U and $U - J$, respectively. DFT+ $U+J$ and DFT+ $U+J$ (minority term) refers to the Hubbard corrective functional of Himmetoglu et al. [46] excluding and including the minority spin term, respectively. The localized-jmDFT (l-jmDFT) functional refers to the localized subspace application corrective functional of Bajaj et al. [47, 48], in which the use of different functional forms for different flat-plane tiles was pioneered. It is applied in this work using U and J parameters evaluated via the simple 2×2 method, which is not how the functional was originally intended to be applied.

Uncorrected approximate DFT, using the PBE approximation, yielded errors in the total energy as high as 232 mHa. Application of Dudarev’s 1998 DFT+ U corrective functional significantly worsened these total energies, yielding errors as high as 682 mHa. This result suggests that Dudarev’s DFT+ U functional, the most widely used Hubbard corrective functional in the literature, does not yield reliable total energies. By comparison, our newly developed mBLOR functional significantly improved upon the raw DFT total energies, with relative errors below 39 mHa across all three test systems.

The original BLOR functional of Eq. 5 improved the total energies over raw DFT (PBE) in some cases but

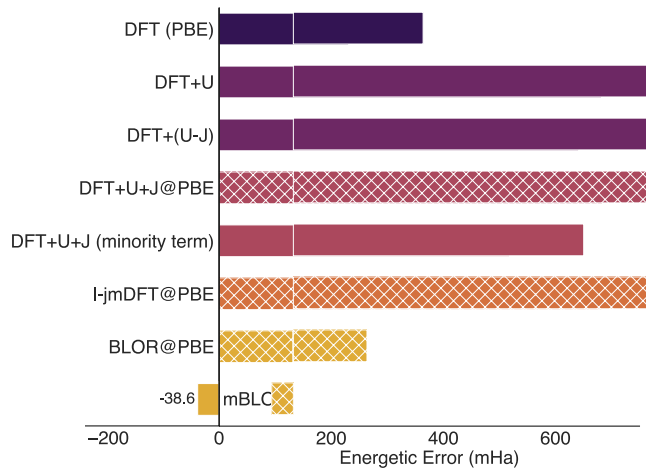


FIG. 3. Bar chart of the errors in the total energy of singlet N_2 at an inter-nuclear separation length of $7a_0$ using different corrective functionals [28, 44, 46–48]. The hashing on the DFT+ $U+J$, l-jmDFT and BLOR bars is used to indicate that these functionals were evaluated non-self consistently using the PBE density, as self-consistent application of these functionals (in a non-spin polarized DFT calculation), results in a symmetry broken ground state charge density. To avoid spurious spin-symmetry breaking, all other corrective functionals were evaluated self-consistently via a non-spin polarized DFT calculation. The raw DFT calculations were performed with the PBE functional [10]. The U and J parameters were evaluated using the simple 2×2 method [33] and U^σ was computed via Eq. 8. All energetic errors are reported relative to twice the DFT(PBE) total energy of the symmetry broken nitrogen atom.

notably worsens the total energy compared to raw DFT for the non-spin polarized O_2 molecule, yielding an energy error of 283 mHa. The success of the mBLOR functional over the original BLOR functional suggests that inter-orbital interactions cannot be neglected in the development of DFT+ U -type functionals that yield reliable total energies, although there may of course prove to be cases where BLOR outperforms mBLOR. The present bar charts show that only the mBLOR DFT+ U functional reduces the error in the raw DFT total energies across all three test systems.

VII. TILTED-PLANE BASED FUNCTIONAL INCLUDING INTER-ORBITAL CORRECTIONS FOR MANY-BODY ERRORS: MBLOR

We are now ready to expand on our previous arguments and derive the mBLOR functional which can be applied to either spin polarized or non-spin polarized systems. The functional can also be used to enforce the global tilted plane condition on finite electronic systems that are in an external Zeeman field, or just when treated with spin-symmetry-broken approximate DFT. To derive this corrective functional we can no longer assume that the spurious curvature in the total subspace energy of an

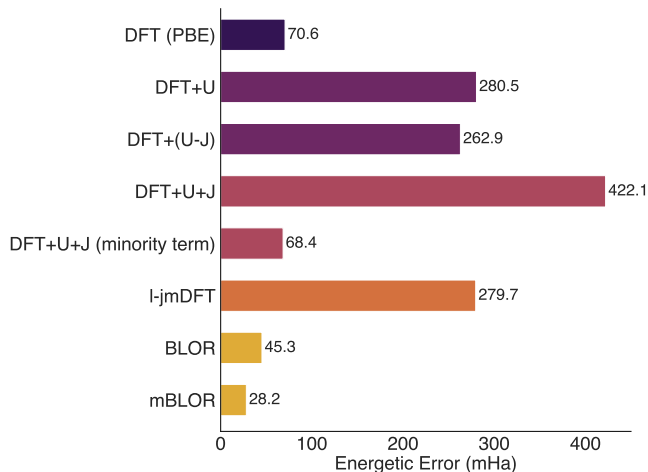


FIG. 4. Bar chart of the errors in the total energy of singlet F_2 at an inter-nuclear separation length of $6a_0$ using different corrective functionals [28, 44, 46–48]. With the exception of the raw DFT(PBE) functional, all total energy errors have been evaluated self-consistently via a non-spin polarized DFT calculation to avoid spurious spin-symmetry breaking. The symmetry unbroken DFT(PBE) calculation failed to converge. The energy error for the DFT(PBE) functional has been evaluated by extrapolating the $DFT+U_{in}$ total energy (for a series of values of U_{in}), back to $U_{in} = 0$. The U and J parameters were evaluated using the simple 2×2 method [33] and U^σ was computed via Eq. 8. All energetic errors are reported relative to twice the DFT(PBE) total energy of the symmetry broken fluorine atom.

approximate XC functional with respect to spin up subspace occupancy n^\uparrow , is equal to the spurious curvature in the total subspace energy with respect to spin down subspace occupancy n^\downarrow . We denote these curvatures simply as U^\uparrow and U^\downarrow , respectively. Now that $U^\uparrow \neq U^\downarrow$, the isosceles trapezoid shaped planes in the $E[N, M]$ energy surface of Fig. 1 will, in the simplest case, fracture into two triangular shaped planes. The breaking of this spin symmetry may be thought of as being due to an effective magnetic field $B_{xc}(\mathbf{r})$, acting on the subspace and due to the surrounding spin polarized material environment. This effective magnetic field is due to the differing spin resolved exchange-correlation potentials, and given by

$$B_{xc}(\mathbf{r}) = \frac{1}{2} (v_{xc}^\uparrow(\mathbf{r}) - v_{xc}^\downarrow(\mathbf{r})), \quad (20)$$

in atomic units. A large variety of different $E[N, M]$ surfaces can arise due to this fracturing. In this study we consider only the simplest case, where each isosceles trapezoid shaped plane fractures into two triangular shaped planes, as presented in Appendix I. This fracturing pattern will occur if the subspace satisfies the following three criteria.

- (a) The total energy of the subspace obeys the strong convexity condition with respect to electron count,

$$2E[N, -M_j] < E[N - 1, M_i] + E[N + 1, M_k], \quad (21)$$

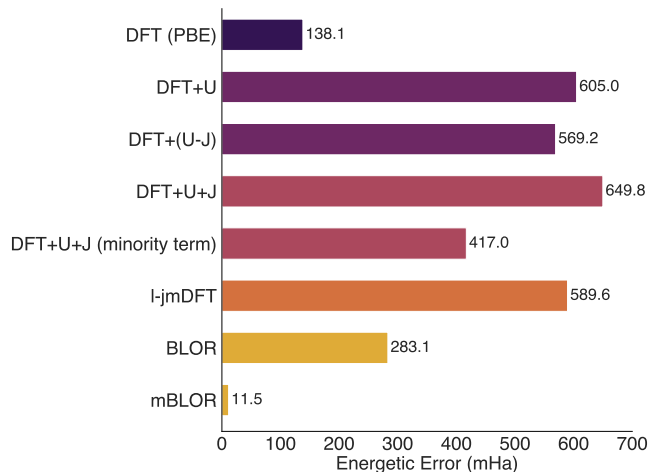


FIG. 5. Bar chart of the errors in the total energy of non-spin polarized O_2 at an inter-nuclear separation length of $6a_0$ using different corrective functionals [28, 44, 46–48]. To simulate the non-spin polarized O_2 molecule, the spin up and spin down occupancies of the doubly degenerate GKS orbitals at the Fermi level were all set equal to 0.5. The raw DFT calculations were performed with the PBE functional [10]. The U and J parameters were evaluated using the simple 2×2 method [33] and U^σ was computed via Eq. 8. The ground state PBE total energy and spin resolved subspace occupancies were evaluated by linearly extrapolating the results from the O_2 calculations with a $DFT+U+J$ -type stabilising potential back to $U_{in} = J_{in} = 0$, see Appendix II for further details. Self-consistent application of the corrective functionals via non-spin polarized DFT calculations results in symmetry broken ground state charge densities, and so for this system the corrective functionals have been evaluated non-self consistently using the extrapolated PBE density. All energetic errors are reported relative to twice the DFT(PBE) total energy of the symmetry broken oxygen atom.

where M_i , M_j , and M_k are the lowest energy magnetization states of the subspace with integer occupancies $N - 1$, N and $N + 1$.

- (b) The subspace-bath interaction energy varies linearly with spin-resolved occupancy.
- (c) Vertices in the subspace energy surface occur only when $M = \pm M_0$, where M_0 is the maximum magnetization of the subspace for a given integer value of occupancy. There exists $4\text{Tr}[\hat{P}]$ such vertices for a given subspace.

In order to enforce the localized tilted plane condition once on an entire multi-orbital subspace that meets criteria (a)-(c), the mBLOR functional is designed to satisfy four key conditions. It must:

1. Be a continuous function of the subspace electron count N and subspace magnetization M .
2. Yield no correction at the $4\text{Tr}[\hat{P}]$ vertices. This is desirable because reasonable approximate function-

als are expected to yield accurate total energies in this case.

3. Have a constant curvature of $-U^\sigma$ with respect to n^σ . This is desirable because approximate functionals are expected to have a spurious curvature of U^σ with respect to n^σ due to their deviation from the localized flat plane condition, and this should be subtracted off.

4. Have a constant curvature of J with respect to M . This is desirable because approximate functionals are expected to have a spurious curvature of $-J$ with respect to M (the minus is due to long-standing convention for defining J), and again this should be subtracted off.

The mBLOR functional is the mathematically unique functional that satisfies these four key conditions, and it is given for each site by

$$E_{\text{mBLOR}} = \begin{cases} \frac{U^\uparrow + U^\downarrow}{4} [(N - N_0) - (N - N_0)^2] + \frac{J}{2} [M^2 - N^2] + \frac{U^\uparrow - U^\downarrow}{4} F_{\text{AMSIE}}^{\text{early}}, & N \leq \text{Tr}[\hat{P}], \\ \frac{U^\uparrow + U^\downarrow}{4} [(N - N_0) - (N - N_0)^2] + \frac{J}{2} [M^2 - (N - 2\text{Tr}[\hat{P}])^2] + \frac{U^\uparrow - U^\downarrow}{4} F_{\text{AMSIE}}^{\text{late}}, & N > \text{Tr}[\hat{P}], \end{cases} \quad (22)$$

which generates the corresponding terms in the spin-dependent potential

$$\hat{v}_{\text{mBLOR}}^\sigma = \begin{cases} \frac{U^\uparrow + U^\downarrow}{4} [1 - 2(N - N_0)] \hat{P} - 2JN^\sigma \hat{P} + \frac{U^\uparrow - U^\downarrow}{4} \hat{v}_{\text{AMSIE}}^{\sigma \text{ early}}[N, M], & N \leq \text{Tr}[\hat{P}], \\ \frac{U^\uparrow + U^\downarrow}{4} [1 - 2(N - N_0)] \hat{P} - 2J [N^\sigma - \text{Tr}[\hat{P}]] \hat{P} + \frac{U^\uparrow - U^\downarrow}{4} \hat{v}_{\text{AMSIE}}^{\sigma \text{ late}}[N, M], & N > \text{Tr}[\hat{P}]. \end{cases} \quad (23)$$

Here, N^σ is the subspace occupancy for the opposite spin channel to that indexed by σ . The unitless quantity $F_{\text{AMSIE}}[N, M]$ is here termed the asymmetric-many electron self interaction error function and $\hat{v}_{\text{AMSIE}}^\sigma[N, M]$ is the correspondingly generated spin- σ asymmetric-MSIE potential operator. These are defined in Appendix I. The $F_{\text{AMSIE}}[N, M]$ function arises whenever $U^\uparrow \neq U^\downarrow$. In such cases, a spin-symmetric and spin-asymmetric term is needed to properly mitigate the localized many electron self interaction error. A demonstration of how functionals of this general type are derived, and then proven to be unique, is provided in Supplementary Materials S-I and S-II of Ref. 28. The asymmetric-MSIE term has already been studied for s-valence systems by Burgess et al. [28] and its inclusion was found to be necessary for yielding accurate total energies for the stretched triplet H_5^+ ring system. The eight different forms of the asymmetric-MSIE function are presented in Appendix I along with the corresponding Asymmetric-MSIE potential operators.

It is worth emphasizing that for non-spin polarized systems the mBLOR functional of Eq. 22 simplifies to the spin symmetric functional of Eq. 18. Furthermore, in the case of single orbital subspaces, Eq. 22 is equivalent to the original BLOR functional, which unlike standard DFT+ U functionals has been shown to yield accurate total energies for dissociated s-valence molecules, namely H_2 , He_2^+ , Li_2 , Be_2^+ and triplet H_5^+ .

It is worth mentioning that the implementation of the mBLOR functional does not require substantial modifications to an existing simplified rotationally invariant DFT+ U code. Terms in the energy that ordinarily look like $\text{Tr}[\hat{n}^\sigma \hat{n}^{\sigma'}]$ are converted to the form $\text{Tr}[\hat{n}^\sigma] \text{Tr}[\hat{n}^{\sigma'}]$, while terms in the potential that ordinarily look like \hat{n}^σ are converted to the form $N^\sigma \hat{P}$. If starting, as we have, with a code equipped with simplified rotationally invariant DFT+ U + J together with ‘ α ’ and ‘ β ’ potential shifts (that may of course be put to use other than for perturbation), then the aforementioned, along with the provision for spin-dependent Hubbard U parameters, is all the in-code modification that is strictly needed for mBLOR. The rest can be done by parameter rearrangement externally. This is even more so the case for the spin-symmetric approximation to BLOR, which requires no code modification at all given a rotationally-invariant DFT+ U starting point, as discussed in the SM of Ref. 28.

VIII. SPIN-ASYMMETRIC MOLECULAR TEST

In the case of the singlet N_2 , F_2 and non-spin polarized O_2 molecules, the mBLOR functional of Eq. 22 simplifies to the spin symmetric mBLOR functional, which has been shown to yield energy errors below 39 mHa across these three test systems. The stretched Ne_2^+ molecule was selected as a spin-polarized test system for

the mBLOR functional due to its potential for harboring both symmetric and asymmetric SIE in their many-body forms. Unlike the singlet N_2 , F_2 and non-spin polarized O_2 molecules, at large inter-nuclear separation lengths a non-integer number of electrons (approximately 5.5 electrons) will localize on each of the two atomic sites and hence the system will suffer from localized-MSIE. The atomic subspaces of the Ne_2^+ molecule are maximally spin polarized and so the system is expected to suffer from negligible localized-SCE. Mori-Sánchez et al. [27] have shown that standard DFT functionals either yield accurate total energies for the stretched H_2^+ molecule, which is dominated by localized MSIE, or accurate total energies for the stretched H_2 molecule, which is dominated by localized SCE, but never accurate total energies for both systems (of course some DFT functionals perform poorly for both). These four molecules at large separation lengths are therefore challenging test cases for any DFT+ U -type functional, as in order to yield reliable total energies across all four test systems, the DFT+ U functional must be able to mitigate both forms of error.

In the dissociated limit the total energy of a cationic dimer X_2^+ should converge to the sum of the energies of the X atom and cation, in what might be considered the generalized extensivity condition

$$E[X_2^+] = E[X] + E[X^+]. \quad (24)$$

As was the case with the non-spin polarized test systems, we use the PBE total energies from the right-hand side of Eq. 24 as our reference value, i.e., the sum of the PBE X atom and X^+ cation total energies. The bar chart of the energy errors associated with each DFT+ U -type functional are presented in Fig. 6.

As shown in the bar chart of Fig. 6, the raw PBE functional yields an energy error of 111 mHa and application of other DFT+ U -type functionals significantly worsens this total energy, with the exception of BLOR and mBLOR. The appropriate mBLOR functional reduces the PBE energy error to only -2.5 mHa. The original BLOR functional also performs exceptionally well for this test system, yielding an energy error of only -4.4 mHa. The success of the original BLOR functional in this particular test system is attributed to the fractional occupancy at the atomic site being limited to a single orbital, with the other two orbitals being almost fully occupied.

When applying the mBLOR functional to spin polarized systems, as was the case for non-spin polarized systems, one must choose between the ‘early’ and ‘late’ versions of the mBLOR functional. In the case of the stretched Ne_2^+ molecule, the subspace is significantly more than half occupied ($N \approx 5.5$) and thus the ‘late’ version of the functional should be applied. For spin polarized systems, one must also choose the correct AMSIE function, of which there are eight. The eight different forms of the AMSIE function are given in Appendix I, along with a practical selection procedure to ensure the correct AMSIE function is chosen for a given subspace.

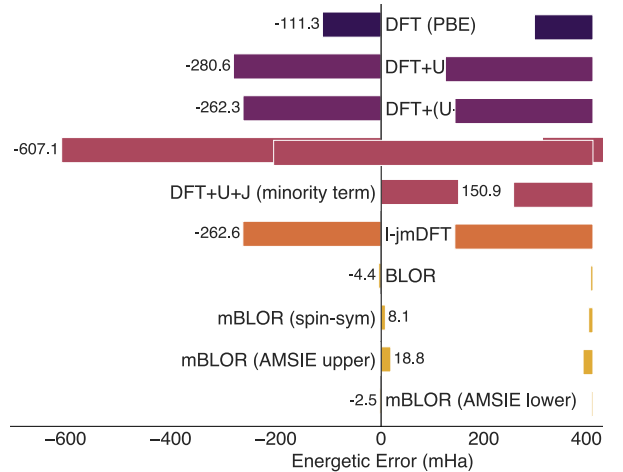


FIG. 6. Bar chart of the errors in the total energy of the doublet Ne_2^+ molecule at an inter-nuclear separation length of $5a_0$ using different corrective functionals [28, 44, 46–48]. The raw DFT calculations were performed with the PBE exchange correlation functional [10]. The energy errors for the Hubbard type corrective functionals reported in this bar chart have been evaluated non-self consistently using the PBE density as all self consistent corrective functional calculations failed to converge for this system, with the notable exception of the mBLOR functional. All energetic errors are reported relative to the sum of the DFT(PBE) total energies of the neon atom and its spin-symmetry broken cation.

In the case of the stretched Ne_2^+ molecule, the most important step in the AMSIE function selection procedure is choosing between the ‘lower’ and ‘upper’ versions of the AMSIE function. Both correctly yield no energy correction when the subspace occupancy is equal to that of the neutral neon atom, i.e., $N = 6$ and $M = 0$, but only the ‘lower’ version of the AMSIE function yields no energy correction when the spin resolved subspace occupancy is equal to that of the spin polarized neon cation, i.e., $N = 5$ and $M = \pm 1$. The ‘lower’ version of the AMSIE function is thus the correct version to apply to this molecular system. Unsurprisingly, it yielded the smallest energy error of -2.5 mHa. If one instead choose (incorrectly) to apply the ‘upper’ version of the AMSIE function, the energy error increases to 18.8 mHa (when also we incorrectly set $U^\uparrow > U^\downarrow$). Alternatively, choosing to omit the AMSIE function and instead apply the spin-symmetric mBLOR functional with $U^\uparrow = U^\downarrow = f^{\uparrow\downarrow}$, yields an energy error of 8.1 mHa.

The mBLOR functional is thus the only Hubbard type corrective functional that yielded low energy errors across all four test systems. The significantly improved total energies offered by the mBLOR corrective functional may facilitate the reliable prediction of chemical properties of transition metal compounds that have proven particularly challenging for current DFT+ U -type functionals, such as spin-state energies [99, 100], Heisenberg exchange coupling [101] and surface formation energies [102] but these are avenues for future research.

IX. POTENTIALIZED EXPLICIT DERIVATIVE DISCONTINUITIES FOR THEIR CONVENIENT MANIFESTATION IN THE GENERALIZED KOHN- SHAM BANDGAP

The mBLOR functional of Eq. 22 will exhibit derivative discontinuities [27, 103–108] at integer values of subspace occupancy due to the functional’s explicit dependence on N . Therefore, it is neither a differentiable functional of the electron density or the first-order non-interacting density matrix. The mBLOR functional thus fits into category D of Yang et al.’s [105] functional classification scheme, which is defined as any “*functional of the density or first-order density matrix with explicit discontinuity.*” This derivative discontinuity Δ_{xc}^N , will contribute to the quasi-particle bandgap, Δ , whenever increasing the global electron count N_{tot} by one causes the subspace occupancy at any of the atomic sites to increase through an integer value, so that $[N] = N_0$ also increases by one. This contribution to the quasi-particle bandgap Δ_{xc}^N , will not appear in the Kohn-Sham gap Δ_{KS} or the Generalized Kohn-Sham gap Δ_{GKS} , unless something is done. This is unlike the situation in DFT+ U functionals such as the Dudarev simplified rotationally-invariant one, as those comprise only *implicit* derivative discontinuities via their subspace projected density-matrix dependence (those which give the gap opening of order $U - J$ in GKS). An implicit derivative discontinuity may arise in mBLOR due to possibly different subspace projection weightings at the valence (occupied) and conduction (virtual) band edges, and this is expected to be a small effect for most applications of interest. However, substantial *explicit* derivative discontinuities appear in mBLOR, due to both the N_0 terms and to switch between early and late version, and these are rather unusual in the approximate or corrective functional contexts.

Ordinarily, calculating the mBLOR fundamental gap would not be strictly possible only via the single-particle eigenspectrum, because explicit derivative discontinuities do not manifest there, but it would instead require adding a separate contribution to the bandgap post hoc, as in

$$\Delta = \Delta_{\text{GKS}} + \Delta_{\text{xc}}^N. \quad (25)$$

Even this seems difficult as, opposed to being a constant global derivative discontinuity, the derivative discontinuity of the mBLOR functional is a non-local operator in character (non-local in the sense of exhibiting more than one spatial argument) and more generally a sum over sites of those. For a single site, we may write

$$\hat{\Delta}_{\text{xc}}^N = \tilde{\Delta}_{\text{xc}}[N] \hat{P}. \quad (26)$$

The $\tilde{\Delta}_{\text{xc}}$ function of Eq. 26 itself depends on the subspace

occupancy N . For subspaces with $U^\uparrow \geq U^\downarrow$, we have

$$\tilde{\Delta}_{\text{xc}} = \begin{cases} U^\downarrow - \frac{U^\uparrow - U^\downarrow}{2} N_0, & N < \text{Tr}[\hat{P}], \\ U^\uparrow + 2J\text{Tr}[\hat{P}] - \frac{U^\uparrow - U^\downarrow}{2} \text{Tr}[\hat{P}], & N = \text{Tr}[\hat{P}], \\ U^\uparrow - \frac{U^\uparrow - U^\downarrow}{2} (2\text{Tr}[\hat{P}] - N_0), & N > \text{Tr}[\hat{P}], \end{cases} \quad (27)$$

when N crosses integer values, at which we use $N_0 = N - 1$. For non-spin polarized systems $\tilde{\Delta}_{\text{xc}} = U^\sigma = U - J$, except at half filling. The apparently larger than might be expected contribution of $\tilde{\Delta}_{\text{xc}}$ to the bandgap at subspace half filling ($N = \text{Tr}[\hat{P}]$) is explained in the Bandgap Analysis section. For concision, we do not consider here the more involved forms of $\tilde{\Delta}_{\text{xc}}$ that arise when moving from ‘lower’ to ‘upper’ type tiles at fixed N_0 .

Accounting for the Δ_{xc}^N contribution to the quasi-particle band-gap post calculation would be a rather disappointing if necessary, given that one of the most prominent and convenient features of conventional DFT+ U is that its derivative discontinuity manifests automatically in the Generalized Kohn-Sham bandgap. To solve this and restore the convenient bandgap opening in the GKS eigensystem, we have found that it is possible to ‘potentialize’ the mBLOR explicit derivative discontinuity, that is to represent it as an additional term in the potential. As the derivative discontinuity arises when adding an additional electron to the neutral system, only the conduction band should be affected by this potential. The additional term that achieves a shift of $\tilde{\Delta}_{\text{xc}}[N]$ to the portion of the conduction band that projects onto the localized subspace is

$$\hat{v}_{\Delta_{\text{xc}}}^\sigma = \tilde{\Delta}_{\text{xc}}[N] (1 - \hat{\rho}) \hat{P} (1 - \hat{\rho}), \quad (28)$$

The corresponding energy term may be found, by integration, and it is

$$\begin{aligned} E_{\Delta_{\text{xc}}} &= \frac{1}{2} \tilde{\Delta}_{\text{xc}}[N] \text{Tr} \left[\left(\hat{\rho} - \frac{\hat{\rho}^2}{2} \right) \hat{P} (1 - \hat{\rho}) \right. \\ &\quad \left. + (1 - \hat{\rho}) \hat{P} \left(\hat{\rho} - \frac{\hat{\rho}^2}{2} \right) \right] \\ &= \frac{1}{2} \tilde{\Delta}_{\text{xc}}[N] \text{Tr} \left[\hat{P} (2\hat{\rho} - 3\hat{\rho}^2 + \hat{\rho}^3) \right]. \end{aligned} \quad (29)$$

This yields a vanishing correction to the total energy under the assumption that $\hat{\rho} = \hat{\rho}^2$, which holds for insulators at zero temperature as well as for molecules with non-degenerate ground states. In practice, we have found as long as the initial guess for the electronic structure exhibits a gap, it is possible to apply the $\hat{v}_{\Delta_{\text{xc}}}^\sigma$ self-consistently without adding the vanishing $E_{\Delta_{\text{xc}}}$ to E_{mBLOR} at all, without appreciable loss of convergence

$\Delta\epsilon_{\text{LUMO}}$	$\Delta\epsilon_{\text{HOMO}}$	$\tilde{\Delta}_{\text{xc}}[N]$	Δ
$\frac{1}{2}U$	$\frac{1}{2}U + 10J$	$U + 10J$	U

TABLE I. A summary of the effect of the mBLOR corrective functional on a homo-nuclear spin polarized d-orbital system at half occupancy to first-order perturbation theory. $\Delta\epsilon_{\text{LUMO}}$ and $\Delta\epsilon_{\text{HOMO}}$ denote the shift to the lowest unoccupied and highest occupied GKS eigenvalues excluding the affect of the $\tilde{\Delta}_{\text{xc}}[N]$ term. The third column presents the gap opening due to the $\tilde{\Delta}_{\text{xc}}[N]$ term and finally Δ denotes the mBLOR functional's total contribution to the GKS gap.

performance. Of course, for finite-temperature systems, metals, or degenerate molecules, it would be necessary to add $E_{\Delta_{\text{xc}}}$ to the energy, for consistency.

X. BANDGAP ANALYSIS

To illustrate the corrective nature of the mBLOR functional, we may consider its application to a homo-nuclear spin-polarized system of transition metal atoms at half occupancy, so that each atomic d-orbital subspace is occupied by five spin up electrons and zero spin down electrons. For simplicity assume that the total subspace occupancy is infinitesimally greater than five and $U^\uparrow = U^\downarrow = U$, so that the late version of the mBLOR functional is applied and the $F_{\text{AMSIE}}^{\text{late}}[N, M]$ function can be neglected. Furthermore, assume that the highest occupied and lowest unoccupied GKS orbitals project perfectly onto the atomic subspace. The spin-up subspace is maximally occupied so that the highest occupied GKS eigenvalue (ϵ_{HOMO}) is spin-up and the lowest unoccupied GKS eigenvalue (ϵ_{LUMO}) is spin-down.

In this particular example, the subspace is at a vertex in the $E[N, M]$ surface and so, to first-order in perturbation theory, the mBLOR corrective functional offers no correction to the total energy. If we now turn our attention to the potential. Excluding the $\tilde{\Delta}_{\text{xc}}[N]$ term, application of the mBLOR corrective functional will, to first order perturbation theory, shift the highest occupied GKS eigenvalue by

$$\Delta\epsilon_{\text{HOMO}} = \frac{U}{2} + 10J, \quad (30)$$

and shift the lowest unoccupied GKS eigenvalue by

$$\Delta\epsilon_{\text{LUMO}} = \frac{U}{2}. \quad (31)$$

This results in a closing of the GKS gap by $10J$, a very surprising result at first. However, the incorporation of the $\tilde{\Delta}_{\text{xc}}[N]$ term will counteract this affect precisely, by opening the gap by order $U + 10J$, resulting in an effective gap opening of U . These results are summarized in Table I.

While further testing will be needed, based on the systems tested here, the mBLOR functional may offer

improved bandgaps over other DFT+ U -type functionals. In the case of the stretched N_2 and F_2 molecules, the mBLOR functional is found to be the only known DFT+ U functional to open the bandgap appreciably. In these systems an approximately integer number of electrons localizes on each atomic site, so we employ the derivative discontinuity correction term when applying the mBLOR functional. In the stretched N_2 system the subspace occupancy is approximately equal to 3.0 and so we let $\tilde{\Delta}_{\text{xc}}[N] = U^\uparrow + 6J$ and in the stretched F_2 system the subspace occupancy is approximately equal to 5.0 and so we let $\tilde{\Delta}_{\text{xc}}[N] = U^\uparrow$, where we recall that $U^\uparrow = U^\downarrow$ in these spin symmetric systems. The raw DFT calculation at the PBE level yields a gap of only 0.06 eV and 0.28 eV, respectively, for N_2 and F_2 . Application of other DFT+ U -type functionals including Dudarev's 1998 Hubbard functional and the original BLOR functional fail to improve the poor PBE result. In contrast, the mBLOR functional opens the gap to 11.92 eV and 9.42 eV, respectively. These bandgaps are still smaller than the anticipated values of 14.60 and 14.02 eV, but this represents an improvement by over one-order of magnitude compared to all other DFT+ U functionals tested here. The anticipated values are based on the assumption that the fundamental bandgap of the stretched N_2 and F_2 molecules are at the dissociated limit, in which case the gap will be equal to that of the isolated nitrogen or fluorine atom, respectively. These results are presented in Fig 7.

The failure of Dudarev's functional to improve the bandgap prediction for the stretched, symmetry unbroken N_2 and F_2 molecules compared to raw DFT is not a result unique to these two molecules, in fact Dudarev's functional will fail to open the bandgap of any symmetry unbroken, stretched, neutral, homo-nuclear dimer. This can be readily explained using the stretched H_2 molecule. At these large inter-nuclear separation lengths, the highest occupied and lowest unoccupied GKS orbitals can be approximated as a linear combination of the hydrogenic atomic orbitals centred at the atomic sites 1 and 2,

$$|\psi_{\text{GKS}}\rangle = \frac{1}{\sqrt{2}} (|\psi_1\rangle \pm |\psi_2\rangle), \quad (32)$$

and the spin resolved GKS density operator is

$$\hat{\rho}^\sigma = \frac{1}{2} (|\psi_1\rangle \langle\psi_1| + |\psi_1\rangle \langle\psi_2| + |\psi_2\rangle \langle\psi_1| + |\psi_2\rangle \langle\psi_2|). \quad (33)$$

Dudarev's functional contributes an additional term to the GKS potential,

$$\hat{v}_{\text{u}} = \frac{U_{\text{eff}}}{2} \left(\sum_I \hat{P}_I - 2\hat{P}_I \hat{\rho}^\sigma \hat{P}_I \right), \quad (34)$$

where the summation runs over the two atomic sites and \hat{P}_I is the atomic projection operator centred at site I , which in the case of an s-valence system, will be composed of a single atomic orbital

$$\hat{P}_I = |\psi_I\rangle \langle\psi_I|. \quad (35)$$

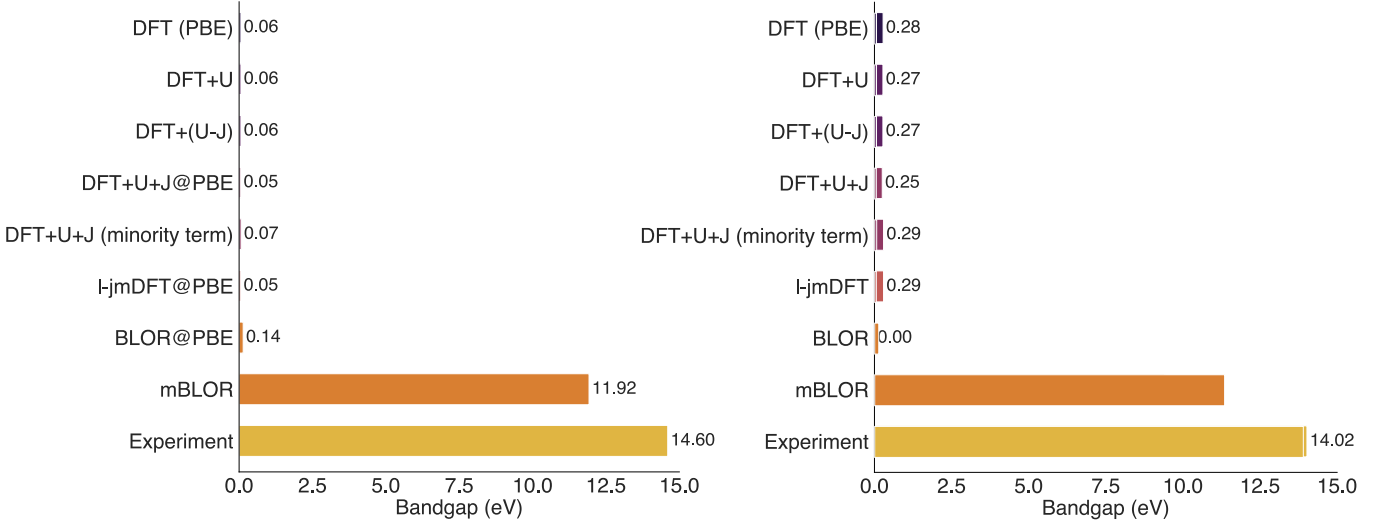


FIG. 7. Bar chart of the predicted bandgaps of the stretched singlet N₂ and F₂ molecules at an inter-nuclear separation length of $7a_0$ and $6a_0$, respectively, using different corrective functionals [28, 44, 46–48]. The PBE exchange correlation functional [10] was employed throughout. With the exception of the mBLOR functional, all bandgap predictions needed to be evaluated via non-spin polarized DFT calculations to avoid spurious spin symmetry breaking. For the N₂ molecule, the DFT+U+J, l-jmDFT and BLOR functionals were evaluated non-self consistently using the PBE density, as self-consistent application of these functionals (in a non-spin polarized DFT calculation), results in a symmetry broken ground state charge density. For the F₂ molecule, the symmetry unbroken DFT(PBE) calculation failed to converge and so the bandgap for the DFT(PBE) functional has been evaluated by extrapolating the DFT+U_{in} bandgap (for a series of values of U_{in}), back to U_{in} = 0. The reference experimental bandgaps for the stretched N₂ and F₂ molecules were assumed to be equal to their respective bandgaps at the dissociated limit and as such were evaluated as the difference between the reference atomic ionization potential [88] and atomic electron affinity [109] of the respective elements. One should note that the reference value for the electron affinity of the nitrogen atom is negative at -0.07 eV.

To first order perturbation theory, Dudarev’s DFT+U correction to the highest occupied GKS eigenvalue is

$$\langle \psi_{\text{HOGKS}} | \hat{v}_u | \psi_{\text{HOGKS}} \rangle = \frac{U_{\text{eff}}}{2} \sum_{IK} \frac{1}{\sqrt{2}} \langle \psi_I | \left(\sum_J \hat{P}_J - 2\hat{P}_J \hat{\rho}^\sigma \hat{P}_J \right) \frac{1}{\sqrt{2}} | \psi_K \rangle, \quad (36)$$

which through use of Eqs 33 & 35 one can readily show is equal to zero assuming the H₂ molecule is sufficiently stretched so that $\langle \psi_I | \psi_J \rangle \approx 0$, when $I \neq J$. Therefore, to first order perturbation theory, Dudarev’s functional will offer no correction to the highest occupied GKS eigenvalue. The same is true for the lowest unoccupied GKS eigenvalue and thus Dudarev’s functional cannot be used to open the GKS gap of the stretched H₂ molecule. The same argument can also be applied to any symmetry unbroken, stretched, neutral, homo-nuclear p-block and d-block dimer (we exclude van der Waals molecules in this discussion), assuming the GKS orbitals are quasi-degenerate at the raw DFT level and can be approximated as an equally weighted linear combination of one p/d orbital centred on each atomic site. To further highlight the failure of conventional DFT+U functional to improve the bandgap of such systems without spurious symmetry breaking, we also present the bandgap of the symmetry unbroken stretched H₂ molecule in Fig 8. By comparison, the mBLOR functional yields a bandgap of

10.67 eV, in close but not perfect agreement with the anticipated value of 12.84 eV.

For the stretched Ne₂⁺ molecule, a non-integer number of electrons localizes on each atomic site ($N \approx 5.5$) and so in this case no derivative discontinuity correction will be applied with the mBLOR functional. The fundamental bandgap of the Ne₂⁺ molecule is equal to the difference in magnitude of the ionization potential and electron affinity,

$$\Delta = (E[\text{Ne}_2^+] - E[\text{Ne}_2^{+2}]) - (E[\text{Ne}_2] - E[\text{Ne}_2^+]). \quad (37)$$

In the dissociated limit, each total energy term in Eq 37 simplifies to the sum of two isolated neon atom/ion energies,

$$\Delta = (E[\text{Ne}] + E[\text{Ne}^+] - 2E[\text{Ne}^+]) - (2E[\text{Ne}] - E[\text{Ne}] - E[\text{Ne}^+]) = 0. \quad (38)$$

Therefore the anticipated value of the bandgap of the stretched Ne₂⁺ is 0 eV, assuming the fundamental bandgap of the Ne₂⁺ molecule at $5a_0$ is at the dissociated limit. The raw DFT calculation at the PBE level yields a bandgap of 0.327 eV and similarly, the mBLOR functional yields a gap of 0.359 eV. These small residual gaps can be attributed to the Ne₂⁺ molecule not completely reaching its dissociated limit at this inter-nuclear separation length.

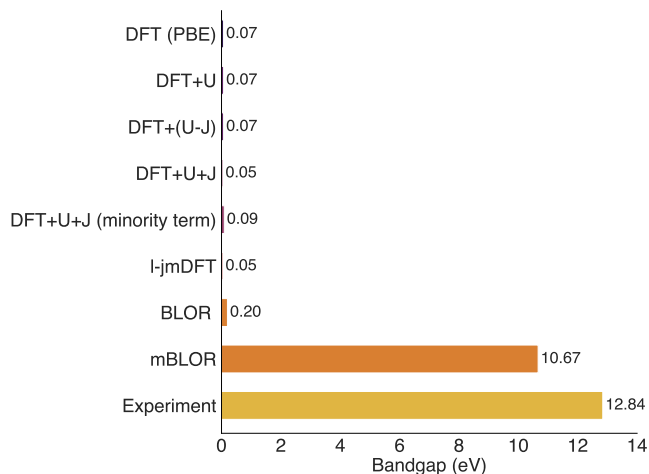


FIG. 8. Bar chart of the predicted bandgaps of the stretched singlet H_2 molecule at an inter-nuclear separation length of $9a_0$ using different corrective functionals [28, 44, 46–48]. The raw DFT calculations were performed with the PBE exchange correlation functional [10]. The DFT+ U and DFT+($U - J$) relative errors were computed using Dudarev et al.’s 1998 functional with the effective Hubbard parameter (U_{eff}) set as U and $U - J$, respectively. The reference experimental bandgap for the stretched H_2 molecule was assumed to be equal to its respective bandgap at the dissociated limit and, as such, was evaluated as the difference between the reference atomic ionization potential [88] and atomic electron affinity [109]. All bandgap predictions were evaluated via spin-polarized DFT calculations, for this system all corrective functionals preserved spin symmetry.

XI. SUBSPACE POPULATION ANALYSIS

By virtue of the mBLOR functional being an explicit functional of the total subspace occupancy N and magnetization M , as opposed to the spin resolved orbital occupancies n_{mm}^{σ} , mBLOR will typically be more sensitive to the choice of projection operator \hat{P} used to define the localized subspace. Very simplistically, we expect the sensitivity of the energy for each subspace to approximately be a factor of $\text{Tr}[\hat{P}]$ times larger than that of BLOR or Dudarev’s functional.

In the case of the highly stretched molecular test systems employed in this study, the atomic orbitals represent an near-ideal choice for the subspace projection operator \hat{P} . However, due to the sensitivity of the mBLOR functional to the subspace population analysis, e.g., to spillage and overlap, future application of this corrective functional to standard molecular and solid state systems in the bonding regime will require careful analysis of the suitability of using the atomic orbitals to define the subspace projection operator, as is standard practice for use with traditional DFT+ U -type functionals. The combination of mBLOR with projectors of Wannier-function type is a very attractive avenue for future exploration.

XII. FUTURE WORK

Future studies are expected to focus on the application of the mBLOR corrective functional to strongly correlated 3d transition metal oxides. For such solid state systems, particular emphasis will need to be given to the mBLOR potential $\hat{v}_{\text{mBLOR}}^{\sigma}$. The relatively large correction offered by the mBLOR potential could significantly alter the electronic structure of the system compared to that of the bare DFT calculation. In particular, the symmetric-MSIE term will drive the subspace towards integer occupancy.

As presented in Eq. 23, the mBLOR potential is defined piecewise with respect to subspace occupancy N , due to its dependence on $N_0 = \lfloor N \rfloor$ and due to the existence of both an early and late version of the functional. This piecewise definition could present convergence issues, particularly if the subspace is driven to integer occupancy, as in such cases a small update in the value of N could change the value of $N_0 = \lfloor N \rfloor$, which will result in a large change to the corrective potential.

The performance of the derivative discontinuity correction term $\hat{v}_{\Delta_{\text{xc}}}^{\sigma}$, when applied to transition metal oxide systems will also need a thorough investigation. In general, the use of this term is advisable, as it will typically be needed to keep the GKS gap open. Due to the presence of the subspace projection operator \hat{P} in Eq. 28, the derivative discontinuity correction will shift only the portion of the conduction band that projects onto the localized subspace. However, the conduction band edge of transition metal oxide systems is often of mixed atomic character and therefore the correct treatment of the bandgap may demand application of the derivative discontinuity correction to, e.g., the oxygen 2p and transition metal 4s atomic subspaces, in addition to the transition metal 3d subspace where the DFT+ U correction is more traditionally applied.

Further investigation and likely refinement of the mBLOR functional will thus be necessary in order for the method to enjoy large-scale adoption. If the promising energetic results obtained for the stretched molecular test systems can be repeated for transition metal oxides, this novel DFT+ U functional could offer a reliable yet computationally inexpensive technique of simulating a suite of physical and chemical properties of transition metal oxide systems that depend on the total energy, such as redox potentials in Li-ion battery cathodes [110–112], surface formation energies for photo-catalysts [102, 113, 114] and crystallographic structures of high T_c superconductors in their normal state [115, 116]. Many challenges and opportunities thus remain in the emerging area of expediently correcting approximate DFT *in situ* using double-counting free generalized Hubbard corrections such as BLOR and mBLOR. The potential intellectual and practical rewards are considerable.

XIII. CONCLUSIONS

A double-counting approximation free DFT+ U -type corrective functional named mBLOR has been derived from first principles to enforce the tilted plane condition on localized, multi-orbital subspaces. This corrective functional is designed to depend only on the total subspace occupancy and magnetization, so that the many-body (inter-orbital including) self-interaction (symmetric and asymmetric) and static correlation errors are addressed in a very cost-effective and easy to implement way. This approach ensures consistency between how subspace-resolved errors are measured, via the Hubbard and Hund parameters, and how they are corrected. The formalism is readily applicable to orbital-free DFT, ensemble DFT, or many other types of electronic structure theory. The mBLOR functional was benchmarked against a variety of other DFT+ U -type functionals using stretched, homo-nuclear, p-block dimers and was the only corrective functional that consistently yielded significantly improved total energies, in this idealized and hence stringent limit for such functionals, when compared to the raw DFT (PBE) values. The mBLOR functional was also the only DFT+ U functional that opened the bandgap of the stretched, spin-symmetric N_2 and F_2 molecules, as well as H_2 , when its explicit derivative discontinuity is ‘potentialized’, a technique that may prove useful in other contexts. Much further study will be needed to understand how the mBLOR (and its progenitor BLOR) functionals perform in applied simulation, both for total-energy and GKS eigenspectrum based properties. Its effect on the potential, in particular, appears to typically be greater in general than from its BLOR or DFT+ U counterparts, due to the inclusion of inter-orbital contributions, and this warrants exploration. Yet the present results are most encouraging, and in general our findings highlight the diagnostic potential of using exact results that hold for idealized yet physical test systems, as well as the promising route of building expedient correctors for approximate DFT using exact conditions such as the tilted-plane condition.

XIV. ACKNOWLEDGMENTS

The research conducted in this publication was funded by the Irish Research Council under grant number GOIPG/2020/1454. All calculations were performed on the Boyle and Kelvin clusters maintained by the Trinity Centre for High Performance Computing. The Boyle cluster was funded through grants from the European Research Council & Science Foundation Ireland and the Kelvin cluster was funded by the Irish National Infrastructure Federation.

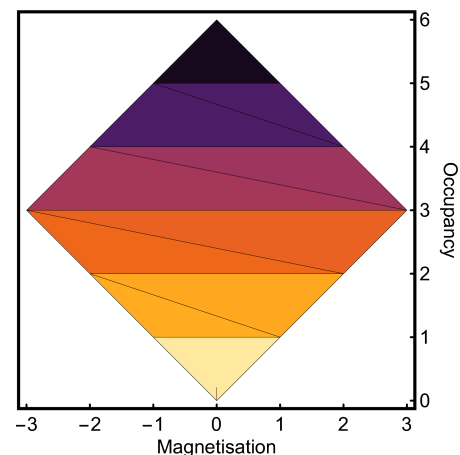


FIG. 9. The fractured $E_v[N, M]$ energy surface for a p-orbital subspace that satisfies criteria (a)-(c), with $U^\uparrow > U^\downarrow$. For ease of visualization, each $N_0 \leq N \leq N_0 + 1$ segment is highlighted a different color. A single line of fracture occurs within each $N_0 \leq N \leq N_0 + 1$ segment, with the exception of the $0 \leq N \leq 1$ and $2\text{Tr}[\hat{P}] - 1 \leq N \leq 2\text{Tr}[\hat{P}]$ segments. The mirror image, through the vertical $M = 0$ line, of this fracturing pattern will occur if $U^\downarrow < U^\uparrow$, while no diagonal fracturing occurs for $U^\uparrow = U^\downarrow$. Over-simplistically, but perhaps helpfully for visualization of the shown $U^\uparrow > U^\downarrow$ example, we can envisage the greater discretized energy curvature in the spin-up direction (which points at 45 degrees up-and-right away from the origin) necessitating additional fracturing along the vertex connection lines that are near-perpendicular to that direction.

XV. APPENDIX I: THE ASYMMETRIC-MSIE FUNCTION

The fracturing pattern for a p-orbital subspace (as an example) that satisfies criteria (a)-(c), as explicated in the derivation of the mBLOR functional is displayed in Fig. 9. The Asymmetric-MSIE function $F_{\text{AMSIE}}[N, M]$, is an explicit function of the subspace occupancy and magnetization but it has eight different forms. The following three criteria can be used to determine which form of the AMSIE function should be employed for a given subspace.

1. The relative magnitude of U^\uparrow and U^\downarrow . A different version of the AMSIE function should be employed if $U^\uparrow > U^\downarrow$ or vice-versa.
2. If the subspace occupancy is less than half occupied, i.e., $N \leq \text{Tr}[\hat{P}]$, the ‘early’ version of the AMSIE function should be employed. If the subspace is more than half occupied, i.e., $N > \text{Tr}[\hat{P}]$, the ‘late’ version of the AMSIE function is required.
3. The ‘upper’ or ‘lower’ version of the AMSIE function should be employed depending whether the point (N, M) on the N - M plane, where N is the subspace occupancy and M the subspace magnetization, is located above or below the line of fracture

$U^\dagger > U^\downarrow$, lower
$F_{\text{AMSIE}}^{\text{early}} [N, M] = -(N - N_0)(1 + N_0 + M)$
$F_{\text{AMSIE}}^{\text{late}} [N, M] = -(N - N_0)(2\text{Tr}[\hat{P}] - N_0 - 1 + M)$
$U^\dagger > U^\downarrow$, upper
$F_{\text{AMSIE}}^{\text{early}} [N, M] = -(N_0 + 1 - N)(N_0 - M)$
$F_{\text{AMSIE}}^{\text{late}} [N, M] = -(N_0 + 1 - N)(2\text{Tr}[\hat{P}] - N_0 - M)$
$U^\dagger < U^\downarrow$, lower
$F_{\text{AMSIE}}^{\text{early}} [N, M] = (N - N_0)(1 + N_0 - M)$
$F_{\text{AMSIE}}^{\text{late}} [N, M] = (N - N_0)(2\text{Tr}[\hat{P}] - N_0 - 1 - M)$
$U^\dagger < U^\downarrow$, upper
$F_{\text{AMSIE}}^{\text{early}} [N, M] = (N_0 + 1 - N)(N_0 + M)$
$F_{\text{AMSIE}}^{\text{late}} [N, M] = (N_0 + 1 - N)(2\text{Tr}[\hat{P}] - N_0 + M)$

TABLE II. The eight different forms of the Asymmetric-MSIE function, $F_{\text{AMSIE}} [N, M]$.

$\hat{v}_{\text{AMSIE}}^\dagger$	$\hat{v}_{\text{AMSIE}}^\dagger$
$U^\dagger > U^\downarrow$, lower	$U^\dagger > U^\downarrow$, lower
$\hat{v}_{\text{AMSIE}}^{\text{early}} [N, M] = -\hat{P} - 2N^\dagger \hat{P}$	$\hat{v}_{\text{AMSIE}}^{\text{early}} [N, M] = (-2N_0 - 1)\hat{P} + 2N^\dagger \hat{P}$
$\hat{v}_{\text{AMSIE}}^{\text{late}} [N, M] = (2N_0 + 1 - 2\text{Tr}[\hat{P}])\hat{P} - 2N^\dagger \hat{P}$	$\hat{v}_{\text{AMSIE}}^{\text{late}} [N, M] = (1 - 2\text{Tr}[\hat{P}])\hat{P} + 2N^\dagger \hat{P}$
$U^\dagger > U^\downarrow$, upper	$U^\dagger > U^\downarrow$, upper
$\hat{v}_{\text{AMSIE}}^{\text{early}} [N, M] = (1 + 2N_0)\hat{P} - 2N^\dagger \hat{P}$	$\hat{v}_{\text{AMSIE}}^{\text{early}} [N, M] = -\hat{P} + 2N^\dagger \hat{P}$
$\hat{v}_{\text{AMSIE}}^{\text{late}} [N, M] = (1 + 2\text{Tr}[\hat{P}])\hat{P} - 2N^\dagger \hat{P}$	$\hat{v}_{\text{AMSIE}}^{\text{late}} [N, M] = (2\text{Tr}[\hat{P}] - 2N_0 - 1)\hat{P} + 2N^\dagger \hat{P}$
$U^\dagger < U^\downarrow$, lower	$U^\dagger < U^\downarrow$, lower
$\hat{v}_{\text{AMSIE}}^{\text{early}} [N, M] = (1 + 2N_0)\hat{P} - 2N^\dagger \hat{P}$	$\hat{v}_{\text{AMSIE}}^{\text{early}} [N, M] = \hat{P} + 2N^\dagger \hat{P}$
$\hat{v}_{\text{AMSIE}}^{\text{late}} [N, M] = (2\text{Tr}[\hat{P}] - 1)\hat{P} - 2N^\dagger \hat{P}$	$\hat{v}_{\text{AMSIE}}^{\text{late}} [N, M] = (2\text{Tr}[\hat{P}] - 2N_0 - 1)\hat{P} + 2N^\dagger \hat{P}$
$U^\dagger < U^\downarrow$, upper	$U^\dagger < U^\downarrow$, upper
$\hat{v}_{\text{AMSIE}}^{\text{early}} [N, M] = \hat{P} - 2N^\dagger \hat{P}$	$\hat{v}_{\text{AMSIE}}^{\text{early}} [N, M] = (-2N_0 - 1)\hat{P} + 2N^\dagger \hat{P}$
$\hat{v}_{\text{AMSIE}}^{\text{late}} [N, M] = (1 + 2N_0 - 2\text{Tr}[\hat{P}])\hat{P} - 2N^\dagger \hat{P}$	$\hat{v}_{\text{AMSIE}}^{\text{late}} [N, M] = (-2\text{Tr}[\hat{P}] - 1)\hat{P} + 2N^\dagger \hat{P}$

TABLE III. The eight different forms of the spin resolved Asymmetric-MSIE potential operator.

within a given $N_0 \leq N \leq N_0 + 1$ segment. The ‘upper’ version should be employed if it is located above the line of fracture and the ‘lower’ version should be employed if it is located below the line of fracture. No line of fracture occurs in the segment $0 \leq N \leq 1$, in this case the ‘upper’ version should always be employed, similarly no line of fracture occurs in the segment $2\text{Tr}[\hat{P}] - 1 \leq N \leq 2\text{Tr}[\hat{P}]$

and in this case the ‘lower’ version should always be employed.

The eight different forms of the $F_{\text{AMSIE}}[N, M]$ function are listed in table II. The different forms of the spin up and spin down Asymmetric-MSIE potential operator are listed in table III.

XVI. APPENDIX II: COMPUTATIONAL DETAILS

All calculations were performed using the ONETEP (Order-N Electronic Total Energy Package) DFT code [117–120]. The ONETEP code constructs the Kohn-Sham density matrix $\rho(\mathbf{r}, \mathbf{r}')$ from a set of Non-orthogonal Generalized Wannier Functions (NGWFs) $\{\phi_\alpha\}$,

$$\rho(\mathbf{r}, \mathbf{r}') = \sum_{\alpha, \beta} \phi_\alpha(\mathbf{r}) K^{\alpha\beta} \phi_\beta(\mathbf{r}'), \quad (39)$$

where $K^{\alpha\beta}$ is the density kernel. The total energy of the system is minimized by optimizing both $K^{\alpha\beta}$ and $\{\phi_\alpha\}$.

All calculations were completed using the PBE [10] exchange-correlation functional at a high cutoff energy of no lower than 1,500 eV. The dissociated molecular test systems were located in a large simulation cell, no smaller than $70 \times 60 \times 60 a_0^3$, with a Martyna-Tuckerman periodic boundary correction cutoff of $7.0 a_0$ [121].

For a system with N_σ spin σ GKS particles, the occupancy of the lowest N_σ GKS particles was set equal to one, and otherwise set equal to zero. The convergence threshold of the root-mean-square gradient of the density kernel and the NGWFs was set at 1×10^{-6} Ha e^{-1} and 1×10^{-7} Ha $a_0^{3/2}$, respectively, and the electronic energy tolerance was set at 1×10^{-6} eV/atom.

Seven NGWFs were assigned per atom using the split-valence approach for p orbitals, in which case 15% of the norm set to be beyond the matching radius r_m . The NGWF cutoff was set to $14 a_0$. A bespoke set of norm-conserving pseudopotentials with very small cut off radii were made using the OPIUM code [122]. It is important to emphasise that the corrective parameters as well as the subspace occupancies depend strongly on the choice of subspace projection operator \hat{P} . For our purposes we use the atomic orbitals generated using the Pseudoatomic Solver in ONETEP with our bespoke norm-conserving pseudopotentials, specifically the pseudoatomic p-orbitals generated in a neutral non-spin-polarized atomic reference state within the PBE approximation. In the limit of large interatomic separation lengths, the atomic orbitals become an ideal choice for the subspace projection operator, particularly when using PBE atomic reference energies as part of the energy extensivity diagnostic. Thus, by testing the Hubbard functionals on molecular species at large interatomic separation lengths, any resulting errors in the total energies can be attributed to failures in the underlying DFT+ U -type functional as opposed to failures in the subspace projection scheme.

In the case of the stretched singlet N_2 , F_2 and spin-polarized O_2 molecules the raw PBE calculation converged to a spurious spin symmetry broken solution. This results in spin resolved PBE densities that differ qualitatively from the true ground state spin resolved densities of the molecule. This necessitates the evaluation of the Hubbard corrective parameters self-consistently (in the specific sense that we proceed to describe) as the spin resolved densities will change appreciably upon application of a Hubbard type corrective functional.

In the case of the stretched F_2 molecule a series of linear response perturbative calculations were used to evaluate the Hubbard corrective parameters (U_{out} and J_{out}) with Dudarev's DFT+ U functional applied to stabilise the spin symmetry unbroken ground state. The corrective parameters U_{out} and J_{out} were evaluated at a range of values of U_{in} between -18 eV and -22 eV, where U_{in} is the input value of the Hubbard U parameter used in Dudarev's DFT+ U functional to stabilise the spin symmetry unbroken ground state. The self-consistent Hubbard U and Hund's J corrective parameters were found by linearly extrapolating the values of U_{out} and J_{out} back to $U_{\text{in}} = 0$ eV. The same procedure was also implemented for the stretched N_2 and O_2 molecules. However, for these systems the DFT+ U + J functional without the minority spin term was used to stabilise the symmetry unbroken ground state, with the effective Hubbard U_{in} parameter set equal in magnitude to the Hund's J_{in} parameter. U_{out} and J_{out} were evaluated at a range of values of U_{in} between -8 eV and -12 eV in the case of the N_2 molecule and between -21 eV and -24 eV in the case of the O_2 molecule.

Despite the authors' best efforts, no suitable range in values of U_{in} were found for the O_2 molecule in its spin polarized state that sufficiently stabilized the symmetry unbroken solution to allow linear extrapolation of $U_{\text{out}}(U_{\text{in}})$ back to $U_{\text{in}} = 0$ eV. As a result, the calculations on the O_2 molecule were performed in its non-spin polarized state as a suitable range in values of U_{in} could be found for this system. It was worth noting that the spin polarized and non-spin polarized states of the O_2 molecule should be degenerate in energy as they represent the $m_s = 1$ and $m_s = 0$ values of the molecule in its triplet ground state. In many regards the non-spin polarized state of the stretched O_2 molecule poses a significantly more challenging test case for the mBLOR functional as unlike the spin polarized state, the non-spin polarized state will be located at the point of maximum localized-SCE and being a neutral homonuclear molecule at large separation lengths, their will be negligible localized-MSIE present. The values of the Hubbard corrective parameters for each stretched molecular species is reported in table IV.

	U^\dagger	U^\downarrow	U_{simple}	J_{simple}	Magnetization	Separation Length
H ₂	6.783	6.783	8.689	1.905	0.0	9.0
He ₂ ⁺	-37.961	13.729	-13.837	-1.721	1.0	5.0
Li ₂	7.507	7.507	9.251	1.743	0.0	15.0
Be ₂ ⁺	-11.881	3.988	-4.238	-0.291	1.0	10.0
H ₅ ⁺	9.827	4.536	9.154	1.972	2.0	8.0
N ₂	7.450	7.450	8.189	0.740	0.0	7.0
O ₂	8.156	8.156	9.037	0.881	0.0	6.0
F ₂	10.471	10.471	11.429	0.958	0.0	6.0
Ne ₂ ⁺	-43.872	12.855	-17.384	-1.875	1.0	5.0

TABLE IV. The Hubbard and Hund corrective parameters (eV) for the stretched dimers, evaluated using the minimum tracking linear response methodology (within the simple 2×2 scheme that effectively constrains N while M varies, and vice versa). The total magnetization M (unitless electron count) and inter-nuclear separation length in Bohr radii (a_0) is also reported for each molecular species. For completeness and comparison, we also report the values of the first-principles corrective parameters for the stretched s-block species that were evaluated for testing the BLOR corrective functional [28].

-
- [1] P. Hohenberg and W. Kohn, Inhomogeneous Electron Gas, *Phys. Rev.* **136**, B864 (1964).
- [2] W. Kohn and L. J. Sham, Self-Consistent Equations Including Exchange and Correlation Effects, *Phys. Rev.* **140**, A1133 (1965).
- [3] A. M. Teale, T. Helgaker, A. Savin, C. Adamo, B. Aradi, A. V. Arbuznikov, P. W. Ayers, E. Jan Baerends, V. Barone, P. Calaminici, E. Cancès, E. A. Carter, P. Kumar Chattaraj, H. Chermette, I. Ciofini, T. Daniel Crawford, F. D. Proft, J. F. Dobson, C. Draxl, T. Frauenheim, E. Fromager, P. Fuentealba, L. Gagliardi, G. Galli, J. Gao, P. Geerlings, N. Gidopoulos, P. M. W. Gill, P. Gori-Giorgi, A. Görling, T. Gould, S. Grimme, O. Gritsenko, H. J. Aagaard Jensen, E. R. Johnson, R. O. Jones, M. Kaupp, A. M. Köster, L. Kronik, A. I. Krylov, S. Kvaal, A. Laestadius, M. Levy, M. Lewin, S. Liu, P.-F. Loos, N. T. Maitra, F. Neese, J. P. Perdew, K. Pernal, P. Pernot, P. Piecuch, E. Rebolini, L. Reining, P. Romaniello, A. Ruzsinszky, D. R. Salahub, M. Scheffler, P. Schwerdtfeger, V. N. Staroverov, J. Sun, E. Tellgren, D. J. Tozer, S. B. Trickey, C. A. Ullrich, A. Vela, G. Vignale, T. A. Wesolowski, X. Xu, and W. Yang, DFT exchange: Sharing perspectives on the workhorse of quantum chemistry and materials science, *Phys. Chem. Chem. Phys.* **24**, 28700 (2022).
- [4] J. P. Perdew and A. Ruzsinszky, Fourteen easy lessons in density functional theory, *Int. J. Quantum Chem.* **110**, 2801 (2010).
- [5] S. H. Vosko, L. Wilk, and M. Nusair, Accurate spin-dependent electron liquid correlation energies for local spin density calculations: A critical analysis, *Can. J. Phys.* **58**, 1200 (1980).
- [6] U. von Barth and L. Hedin, A local exchange-correlation potential for the spin polarized case. i, *J. Phys. C: Solid State Phys.* **5**, 1629 (1972).
- [7] J. P. Perdew and Y. Wang, Accurate and simple analytic representation of the electron-gas correlation energy, *Phys. Rev. B* **45**, 13244 (1992).
- [8] J. P. Perdew and A. Zunger, Self-interaction correction to density-functional approximations for many-electron systems, *Phys. Rev. B* **23**, 5048 (1981).
- [9] M. T. Entwistle, M. J. P. Hodgson, J. Wetherell, B. Longstaff, J. D. Ramsden, and R. W. Godby, Local density approximations from finite systems, *Phys. Rev. B* **94**, 205134 (2016).
- [10] J. P. Perdew, K. Burke, and M. Ernzerhof, Generalized Gradient Approximation Made Simple, *Phys. Rev. Lett.* **77**, 3865 (1996).
- [11] C. Lee, W. Yang, and R. G. Parr, Development of the Colle-Salvetti correlation-energy formula into a functional of the electron density, *Phys. Rev. B* **37**, 785 (1988).
- [12] J. P. Perdew, A. Ruzsinszky, G. I. Csonka, O. A. Vydrov, G. E. Scuseria, L. A. Constantin, X. Zhou, and K. Burke, Restoring the Density-Gradient Expansion for Exchange in Solids and Surfaces, *Phys. Rev. Lett.* **100**, 136406 (2008).
- [13] A. D. Becke, Density-functional exchange-energy approximation with correct asymptotic behavior, *Phys. Rev. A* **38**, 3098 (1988).
- [14] P. Verma and D. G. Truhlar, HLE16: A Local Kohn-Sham Gradient Approximation with Good Performance for Semiconductor Band Gaps and Molecular Excitation Energies, *J. Phys. Chem. Lett.* **8**, 380 (2017).
- [15] J. Sun, A. Ruzsinszky, and J. P. Perdew, Strongly Constrained and Appropriately Normed Semilocal Density Functional, *Phys. Rev. Lett.* **115**, 036402 (2015).
- [16] J. M. del Campo, J. L. Gázquez, S. B. Trickey, and A. Vela, A new meta-GGA exchange functional based on an improved constraint-based GGA, *Chemical Physics Letters* **543**, 179 (2012).

- [17] J. Tao, J. P. Perdew, V. N. Staroverov, and G. E. Scuseria, Climbing the Density Functional Ladder: Nonempirical Meta-Generalized Gradient Approximation Designed for Molecules and Solids, *Phys. Rev. Lett.* **91**, 146401 (2003).
- [18] Y. Zhao and D. G. Truhlar, A new local density functional for main-group thermochemistry, transition metal bonding, thermochemical kinetics, and noncovalent interactions, *The Journal of Chemical Physics* **125**, 194101 (2006).
- [19] Y. Wang, X. Jin, H. S. Yu, D. G. Truhlar, and X. He, Revised M06-L functional for improved accuracy on chemical reaction barrier heights, noncovalent interactions, and solid-state physics, *Proc. Natl. Acad. Sci. U.S.A.* **114**, 8487 (2017).
- [20] A. D. Becke, Density-functional thermochemistry. III. The role of exact exchange, *The Journal of Chemical Physics* **98**, 5648 (1993).
- [21] J. P. Perdew, M. Ernzerhof, and K. Burke, Rationale for mixing exact exchange with density functional approximations, *The Journal of Chemical Physics* **105**, 9982 (1996).
- [22] J. P. Perdew, Density functional theory and the band gap problem, *Int. J. Quantum Chem.* **28**, 497 (1985).
- [23] A. Ruzsinszky, J. P. Perdew, G. I. Csonka, O. A. Vydrov, and G. E. Scuseria, Spurious fractional charge on dissociated atoms: Pervasive and resilient self-interaction error of common density functionals, *J. Chem. Phys.* **125**, 194112 (2006).
- [24] A. D. Dutoi and M. Head-Gordon, Self-interaction error of local density functionals for alkali-halide dissociation, *Chem. Phys. Lett.* **422**, 230 (2006).
- [25] J. Nafziger and A. Wasserman, Fragment-based treatment of delocalization and static correlation errors in density-functional theory, *J. Chem. Phys.* **143**, 234105 (2015).
- [26] A. C. Burgess, E. Linscott, and D. D. O'Regan, Tilted-Plane Structure of the Energy of Finite Quantum Systems, *Phys. Rev. Lett.* **133**, 026404 (2024).
- [27] P. Mori-Sánchez and A. J. Cohen, The derivative discontinuity of the exchange-correlation functional, *Phys. Chem. Chem. Phys.* **16**, 14378 (2014).
- [28] A. C. Burgess, E. Linscott, and D. D. O'Regan, DFT+ U -type functional derived to explicitly address the flat plane condition, *Phys. Rev. B* **107**, L121115 (2023).
- [29] Q. Zhao, E. I. Ioannidis, and H. J. Kulik, Global and local curvature in density functional theory, *J. Chem. Phys.* **145**, 054109 (2016).
- [30] The term local could also be used here, but in the DFT context it seems preferable to reserve 'local' to describe variables that depend explicitly upon a single spatial argument.
- [31] V. I. Anisimov, J. Zaanen, and O. K. Andersen, Band theory and Mott insulators: Hubbard U instead of Stoner I , *Phys. Rev. B* **44**, 943 (1991).
- [32] J. Hubbard, Electron Correlations in Narrow Energy Bands, *Proc. R. Soc. Lond. Ser. Math. Phys. Sci.* **276**, 238 (1963), 2414761.
- [33] E. B. Linscott, D. J. Cole, M. C. Payne, and D. D. O'Regan, Role of spin in the calculation of Hubbard U and Hund's J parameters from first principles, *Phys. Rev. B* **98**, 235157 (2018).
- [34] M. Cococcioni and S. de Gironcoli, Linear response approach to the calculation of the effective interaction parameters in the LDA+ U method, *Phys. Rev. B* **71**, 035105 (2005).
- [35] I. Timrov, N. Marzari, and M. Cococcioni, Hubbard parameters from density-functional perturbation theory, *Phys. Rev. B* **98**, 085127 (2018).
- [36] D. S. Lambert and D. D. O'Regan, Use of DFT+ U + J with linear response parameters to predict nonmagnetic oxide band gaps with hybrid-functional accuracy, *Phys. Rev. Res.* **5**, 013160 (2023).
- [37] W. E. Pickett, S. C. Erwin, and E. C. Ethridge, Reformulation of the LDA+ U method for a local-orbital basis, *Phys. Rev. B* **58**, 1201 (1998).
- [38] M. Springer and F. Aryasetiawan, Frequency-dependent screened interaction in Ni within the random-phase approximation, *Phys. Rev. B* **57**, 4364 (1998).
- [39] N. J. Mosey and E. A. Carter, Ab initio evaluation of Coulomb and exchange parameters for DFT+ U calculations, *Phys. Rev. B* **76**, 155123 (2007).
- [40] N. J. Mosey, P. Liao, and E. A. Carter, Rotationally invariant ab initio evaluation of Coulomb and exchange parameters for DFT+ U calculations, *The Journal of Chemical Physics* **129**, 014103 (2008).
- [41] V. I. Anisimov, I. V. Solovyev, M. A. Korotin, M. T. Czyżyk, and G. A. Sawatzky, Density-functional theory and NiO photoemission spectra, *Phys. Rev. B* **48**, 16929 (1993).
- [42] M. T. Czyżyk and G. A. Sawatzky, Local-density functional and on-site correlations: The electronic structure of La₂CuO₄ and LaCuO₃, *Phys. Rev. B* **49**, 14211 (1994).
- [43] A. I. Liechtenstein, V. I. Anisimov, and J. Zaanen, Density-functional theory and strong interactions: Orbital ordering in Mott-Hubbard insulators, *Phys. Rev. B* **52**, R5467 (1995).
- [44] S. L. Dudarev, G. A. Botton, S. Y. Savrasov, C. J. Humphreys, and A. P. Sutton, Electron-energy-loss spectra and the structural stability of nickel oxide: An LSDA+ U study, *Phys. Rev. B* **57**, 1505 (1998).
- [45] D.-K. Seo, Self-interaction correction in the LDA+ U method, *Phys. Rev. B* **76**, 033102 (2007).
- [46] B. Himmetoglu, R. M. Wentzcovitch, and M. Cococcioni, First-principles study of electronic and structural properties of CuO, *Phys. Rev. B* **84**, 115108 (2011).
- [47] A. Bajaj, J. P. Janet, and H. J. Kulik, Communication: Recovering the flat-plane condition in electronic structure theory at semi-local DFT cost, *J. Chem. Phys.* **147**, 191101 (2017).
- [48] A. Bajaj, F. Liu, and H. J. Kulik, Non-empirical, low-cost recovery of exact conditions with model-Hamiltonian inspired expressions in jmDFT, *J. Chem. Phys.* **150**, 154115 (2019).
- [49] M. Shishkin and H. Sato, DFT+ U in Dudarev's formulation with corrected interactions between the electrons with opposite spins: The form of Hamiltonian, calculation of forces, and bandgap adjustments, *J. Chem. Phys.* **151**, 024102 (2019).
- [50] S. L. Dudarev, P. Liu, D. A. Andersson, C. R. Stanek, T. Ozaki, and C. Franchini, Parametrization of LSDA+ U for noncollinear magnetic configurations: Multipolar magnetism in UO₂, *Phys. Rev. Materials* **3**, 083802 (2019).
- [51] V. L. Campo and M. Cococcioni, Extended DFT+ U + V method with on-site and inter-site electronic interac-

- tions, *J. Phys.: Condens. Matter* **22**, 055602 (2010).
- [52] A. G. Petukhov, I. I. Mazin, L. Chioncel, and A. I. Liechtenstein, Correlated metals and the LDA+ U method, *Phys. Rev. B* **67**, 153106 (2003).
- [53] I. V. Solovyev, P. H. Dederichs, and V. I. Anisimov, Corrected atomic limit in the local-density approximation and the electronic structure of d impurities in Rb, *Phys. Rev. B* **50**, 16861 (1994).
- [54] F. Flores, D. Soler-Polo, and J. Ortega, A closed local-orbital unified description of DFT and many-body effects, *J. Phys.: Condens. Matter* **34**, 304006 (2022).
- [55] H. Park, A. J. Millis, and C. A. Marianetti, Density functional versus spin-density functional and the choice of correlated subspace in multivariable effective action theories of electronic structure, *Phys. Rev. B* **92**, 035146 (2015).
- [56] E. R. Ylvisaker, W. E. Pickett, and K. Koepf, Anisotropy and magnetism in the LSDA+ U method, *Phys. Rev. B* **79**, 035103 (2009).
- [57] S. Ryee and M. J. Han, The effect of double counting, spin density, and Hund interaction in the different DFT+ U functionals, *Sci Rep* **8**, 9559 (2018).
- [58] G. C. Moore, M. K. Horton, E. Linscott, A. M. Ganose, M. Siron, D. D. O'Regan, and K. A. Persson, High-throughput determination of Hubbard U and Hund J values for transition metal oxides via the linear response formalism, *Phys. Rev. Mater.* **8**, 014409 (2024).
- [59] J. W. Bennett, B. G. Hudson, I. K. Metz, D. Liang, S. Spurgeon, Q. Cui, and S. E. Mason, A systematic determination of hubbard U using the GBRV ultrasoft pseudopotential set, *Computational Materials Science* **170**, 109137 (2019).
- [60] M. K. Horton, J. H. Montoya, M. Liu, and K. A. Persson, High-throughput prediction of the ground-state collinear magnetic order of inorganic materials using Density Functional Theory, *npj Comput Mater* **5**, 1 (2019).
- [61] V. I. Hegde, C. K. H. Borg, Z. Del Rosario, Y. Kim, M. Hutchinson, E. Antono, J. Ling, P. Saxe, J. E. Saal, and B. Meredig, Quantifying uncertainty in high-throughput density functional theory: A comparison of AFLOW, Materials Project, and OQMD, *Phys. Rev. Materials* **7**, 053805 (2023).
- [62] A. D. Kaplan, M. Levy, and J. P. Perdew, The predictive power of exact constraints and appropriate norms in density functional theory, *Annu. Rev. Phys. Chem.* **74**, 193 (2023).
- [63] J. P. Perdew, R. G. Parr, M. Levy, and J. L. Balduz, Density-Functional Theory for Fractional Particle Number: Derivative Discontinuities of the Energy, *Phys. Rev. Lett.* **49**, 1691 (1982).
- [64] W. Yang, Y. Zhang, and P. W. Ayers, Degenerate Ground States and a Fractional Number of Electrons in Density and Reduced Density Matrix Functional Theory, *Phys. Rev. Lett.* **84**, 5172 (2000).
- [65] P. W. Ayers, The dependence on and continuity of the energy and other molecular properties with respect to the number of electrons, *J Math Chem* **43**, 285 (2008).
- [66] A. C. Burgess, E. Linscott, and D. D. O'Regan, The convexity condition of density-functional theory, *J. Chem. Phys.* **159**, 211102 (2023).
- [67] T. Gál and P. Geerlings, Energy surface, chemical potentials, Kohn–Sham energies in spin-polarized density functional theory, *J. Chem. Phys.* **133**, 144105 (2010).
- [68] A. J. Cohen, P. Mori-Sánchez, and W. Yang, Fractional spins and static correlation error in density functional theory, *J. Chem. Phys.* **129**, 121104 (2008).
- [69] G. K.-L. Chan, A fresh look at ensembles: Derivative discontinuities in density functional theory, *J. Chem. Phys.* **110**, 4710 (1999).
- [70] P. Mori-Sánchez, A. J. Cohen, and W. Yang, Discontinuous Nature of the Exchange–Correlation Functional in Strongly Correlated Systems, *Phys. Rev. Lett.* **102**, 066403 (2009).
- [71] J. P. Perdew and E. Sagvolden, Exact exchange–correlation potentials in spin-density functional theory and their discontinuities at unit electron number, *Can. J. Chem.* **87**, 1268 (2009).
- [72] X. De Vriendt, L. Lemmens, S. De Baerdemacker, P. Bultinck, and G. Acke, Quantifying Delocalization and Static Correlation Errors by Imposing (Spin)Population Redistributions through Constraints on Atomic Domains, *J. Chem. Theory Comput.* **17**, 6808 (2021).
- [73] X. De Vriendt, D. Van Hende, S. De Baerdemacker, P. Bultinck, and G. Acke, Uncovering phase transitions that underpin the flat-planes in the tilted Hubbard model using subsystems and entanglement measures, *J. Chem. Phys.* **156**, 244115 (2022).
- [74] B. G. Janesko, Replacing hybrid density functional theory: Motivation and recent advances, *Chem. Soc. Rev.* **50**, 8470 (2021).
- [75] X. D. Yang, A. H. G. Patel, R. A. Miranda-Quintana, F. Heidar-Zadeh, C. E. González-Espinoza, and P. W. Ayers, Communication: Two types of flat-planes conditions in density functional theory, *J. Chem. Phys.* **145**, 031102 (2016).
- [76] R. Cuevas-Saavedra, D. Chakraborty, S. Rabi, C. Cárdenas, and P. W. Ayers, Symmetric Nonlocal Weighted Density Approximations from the Exchange–Correlation Hole of the Uniform Electron Gas, *J. Chem. Theory Comput.* **8**, 4081 (2012).
- [77] Y. Goshen and E. Kraisler, Ensemble Ground State of a Many-Electron System with Fractional Electron Number and Spin: Piecewise-Linearity and Flat-Plane Condition Generalized, *J. Phys. Chem. Lett.* **15**, 2337 (2024).
- [78] M. Richer, F. Heidar-Zadeh, M. Ríos-Gutiérrez, X. D. e. Yang, and P. W. Ayers, Spin-Polarized Conceptual Density Functional Theory from the Convex Hull, *J. Chem. Theory Comput.* **20**, 4616 (2024).
- [79] A. M. Malek and R. Balawender, Discontinuities of energy derivatives in spin-density functional theory (2013), [arxiv:1310.6918 \[physics\]](https://arxiv.org/abs/1310.6918).
- [80] B. G. Janesko, Multiconfigurational Correlation at DFT + U cost: On-Site Electron–Electron Interactions Yield a Block-Localized Configuration Interaction Hamiltonian, *J. Phys. Chem. A* **128**, 5077 (2024).
- [81] N. Q. Su, C. Li, and W. Yang, Describing strong correlation with fractional-spin correction in density functional theory, *Proc. Natl. Acad. Sci.* **115**, 9678 (2018).
- [82] E. Proynov and J. Kong, Correcting the Charge Delocalization Error of Density Functional Theory, *J. Chem. Theory Comput.* **17**, 4633 (2021).
- [83] J. Kong and E. Proynov, Density Functional Model for Nondynamic and Strong Correlation, *J. Chem. Theory Comput.* **12**, 133 (2016).
- [84] E. R. Johnson and J. Contreras-García, Communica-

- tion: A density functional with accurate fractional-charge and fractional-spin behaviour for s-electrons, *J. Chem. Phys.* **135**, 081103 (2011).
- [85] G. Prokopiou, M. Hartstein, N. Govind, and L. Kronik, Optimal Tuning Perspective of Range-Separated Double Hybrid Functionals, *J. Chem. Theory Comput.* **18**, 2331 (2022).
- [86] F. Zhou and V. Ozolins, A unified treatment of derivative discontinuity, delocalization and static correlation effects in density functional calculations (2018), [arxiv:1710.08973 \[cond-mat\]](https://arxiv.org/abs/1710.08973).
- [87] H. van Aggelen, Y. Yang, and W. Yang, Exchange-correlation energy from pairing matrix fluctuation and the particle-particle random-phase approximation, *Phys. Rev. A* **88**, 030501 (2013).
- [88] A. Kramida, Yu. Ralchenko, J. Reader, and NIST ASD Team, NIST Atomic Spectra Database (ver. 5.10), [Online]. Available: <https://physics.nist.gov/asd> [2023, July 7]. National Institute of Standards and Technology, Gaithersburg, MD. (2022).
- [89] P. Mori-Sánchez, A. J. Cohen, and W. Yang, Many-electron self-interaction error in approximate density functionals, *J. Chem. Phys.* **125**, 201102 (2006).
- [90] I. Dabo, A. Ferretti, N. Poilvert, Y. Li, N. Marzari, and M. Cococcioni, Koopmans' condition for density-functional theory, *Phys. Rev. B* **82**, 115121 (2010).
- [91] G. Borghi, A. Ferretti, N. L. Nguyen, I. Dabo, and N. Marzari, Koopmans-compliant functionals and their performance against reference molecular data, *Phys. Rev. B* **90**, 075135 (2014).
- [92] N. Colonna, R. De Gennaro, E. Linscott, and N. Marzari, Koopmans Spectral Functionals in Periodic Boundary Conditions, *J. Chem. Theory Comput.* **18**, 5435 (2022).
- [93] G. Moynihan, G. Teobaldi, and D. D. O'Regan, A self-consistent ground-state formulation of the first-principles Hubbard U parameter validated on one-electron self-interaction error (2017), [arxiv:1704.08076 \[cond-mat\]](https://arxiv.org/abs/1704.08076).
- [94] O. K. Orhan and D. D. O'Regan, First-principles Hubbard U and Hund's J corrected approximate density functional theory predicts an accurate fundamental gap in rutile and anatase TiO_2 , *Phys. Rev. B* **101**, 245137 (2020).
- [95] S. Berman, A. Zhussupbekova, J. E. Boschker, J. Schwarzkopf, D. D. O'Regan, I. V. Shvets, and K. Zhussupbekov, Reconciling the theoretical and experimental electronic structure of NbO_2 , *Phys. Rev. B* **108**, 155141 (2023).
- [96] E. Macke, I. Timrov, N. Marzari, and L. C. Ciacchi, Orbital-Resolved DFT+ U for Molecules and Solids, *J. Chem. Theory Comput.* **20**, 4824 (2024).
- [97] Y. Mei, Z. Chen, and W. Yang, Exact Second-Order Corrections and Accurate Quasiparticle Energy Calculations in Density Functional Theory, *J. Phys. Chem. Lett.* **12**, 7236 (2021).
- [98] C. Li, X. Zheng, N. Q. Su, and W. Yang, Localized orbital scaling correction for systematic elimination of delocalization error in density functional approximations, *National Science Review* **5**, 203 (2018).
- [99] L. A. Mariano, B. Vlasisavljevich, and R. Poloni, Biased Spin-State Energetics of Fe(II) Molecular Complexes within Density-Functional Theory and the Linear-Response Hubbard U Correction, *J. Chem. Theory Comput.* **16**, 6755 (2020).
- [100] S. Vela, M. Fumanal, J. Cirera, and J. Ribas-Arino, Thermal spin crossover in Fe(II) and Fe(III). Accurate spin state energetics at the solid state, *Phys. Chem. Chem. Phys.* **22**, 4938 (2020).
- [101] L. MacEnulty and D. D. O'Regan, Optimization strategies developed on NiO for Heisenberg exchange coupling calculations using projector augmented wave based first-principles DFT+ U + J , *Phys. Rev. B* **108**, 245137 (2023).
- [102] Q. Zhao and H. J. Kulik, Stable Surfaces That Bind Too Tightly: Can Range-Separated Hybrids or DFT+ U Improve Paradoxical Descriptions of Surface Chemistry?, *J. Phys. Chem. Lett.* **10**, 5090 (2019).
- [103] J. P. Perdew and M. Levy, Physical Content of the Exact Kohn-Sham Orbital Energies: Band Gaps and Derivative Discontinuities, *Phys. Rev. Lett.* **51**, 1884 (1983).
- [104] L. J. Sham and M. Schlüter, Density-Functional Theory of the Energy Gap, *Phys. Rev. Lett.* **51**, 1888 (1983).
- [105] W. Yang, A. J. Cohen, and P. Mori-Sánchez, Derivative discontinuity, bandgap and lowest unoccupied molecular orbital in density functional theory, *J. Chem. Phys.* **136**, 204111 (2012).
- [106] T. Gould and J. Toulouse, Kohn-Sham potentials in exact density-functional theory at noninteger electron numbers, *Phys. Rev. A* **90**, 050502(R) (2014).
- [107] E. Kraisler, M. J. P. Hodgson, and E. K. U. Gross, From Kohn-Sham to Many-Electron Energies via Step Structures in the Exchange-Correlation Potential, *J. Chem. Theory Comput.* **17**, 1390 (2021).
- [108] F. Cernatic, B. Senjean, V. Robert, and E. Fromager, Ensemble Density Functional Theory of Neutral and Charged Excitations, *Top. Curr. Chem.* **380**, 4 (2021).
- [109] J. C. Rienstra-Kiracofe, G. S. Tschumper, H. F. Schaefer, S. Nandi, and G. B. Ellison, Atomic and Molecular Electron Affinities: Photoelectron Experiments and Theoretical Computations, *Chem. Rev.* **102**, 231 (2002).
- [110] M. Shishkin and H. Sato, Challenges in computational evaluation of redox and magnetic properties of Fe-based sulfate cathode materials of Li- and Na-ion batteries, *J. Phys.: Condens. Matter* **29**, 215701 (2017).
- [111] T. Mueller, G. Hautier, A. Jain, and G. Ceder, Evaluation of Tavorite-Structured Cathode Materials for Lithium-Ion Batteries Using High-Throughput Computing, *Chem. Mater.* **23**, 3854 (2011).
- [112] M. Cococcioni and N. Marzari, Energetics and cathode voltages of LiMPO_4 olivines ($M=\text{Fe},\text{Mn}$) from extended Hubbard functionals, *Phys. Rev. Mater.* **3**, 033801 (2019).
- [113] X. Torrelles, G. Cabailh, R. Lindsay, O. Bikondoa, J. Roy, J. Zegenhagen, G. Teobaldi, W. A. Hofer, and G. Thornton, Geometric Structure of $\text{TiO}_2(011)(2 \times 1)$, *Phys. Rev. Lett.* **101**, 185501 (2008).
- [114] M. Batzill, Fundamental aspects of surface engineering of transition metal oxide photocatalysts, *Energy Environ. Sci.* **4**, 3275 (2011).
- [115] E. Been, W.-S. Lee, H. Y. Hwang, Y. Cui, J. Zaanen, T. Devereaux, B. Moritz, and C. Jia, Electronic Structure Trends Across the Rare-Earth Series in Superconducting Infinite-Layer Nickelates, *Phys. Rev. X* **11**, 011050 (2021).
- [116] J. W. Furness, Y. Zhang, C. Lane, I. G. Buda, B. Barbiellini, R. S. Markiewicz, A. u. Bansil, and J. Sun, An

- accurate first-principles treatment of doping-dependent electronic structure of high-temperature cuprate superconductors, *Commun Phys* **1**, 1 (2018).
- [117] J. C. A. Prentice, J. Aarons, J. C. Womack, A. E. A. Allen, L. Andrinopoulos, L. Anton, R. A. Bell, A. Bhandari, G. A. Bramley, R. J. Charlton, R. J. Clements, D. J. Cole, G. Constantinescu, F. Corsetti, S. M.-M. Dubois, K. K. B. Duff, J. M. Escartín, A. Greco, Q. Hill, L. P. Lee, E. Linscott, D. D. O'Regan, M. J. S. Phipps, L. E. Ratcliff, Á. R. Serrano, E. W. Tait, G. Teobaldi, V. Vitale, N. Yeung, T. J. Zuehlsdorff, J. Dziedzic, P. D. Haynes, N. D. M. Hine, A. A. Mostofi, M. C. Payne, and C.-K. Skylaris, The ONETEP linear-scaling density functional theory program, *J. Chem. Phys.* **152**, 174111 (2020).
- [118] C.-K. Skylaris, P. D. Haynes, A. A. Mostofi, and M. C. Payne, Introducing ONETEP: Linear-scaling density functional simulations on parallel computers, *J. Chem. Phys.* **122**, 084119 (2005).
- [119] C.-K. Skylaris, A. A. Mostofi, P. D. Haynes, O. Diéguez, and M. C. Payne, Nonorthogonal generalized Wannier function pseudopotential plane-wave method, *Phys. Rev. B* **66**, 035119 (2002).
- [120] D. D. O'Regan, N. D. M. Hine, M. C. Payne, and A. A. Mostofi, Linear-scaling DFT + U with full local orbital optimization, *Phys. Rev. B* **85**, 085107 (2012).
- [121] G. J. Martyna and M. E. Tuckerman, A reciprocal space based method for treating long range interactions in ab initio and force-field-based calculations in clusters, *J. Chem. Phys.* **110**, 2810 (1999).
- [122] OPIUM: The optimized pseudopotential interface unification module, <https://opium.sourceforge.net>.